NASA TECHNICAL NOTE

NASA TN D-8142

NASA TN D-8142

AN ANALYTICAL STUDY OF TURBULENCE RESPONSES, INCLUDING HORIZONTAL-TAIL LOADS, OF A CONTROL-CONFIGURED VEHICLE WITH RELAXED STATIC STABILITY

Boyd Perry III

Langley Research Center
Hampton, Va. 23665

NATIONAL AERONAUTICS AND SPACE ADMINISTRATION • WASHINGTON, D. C. • FEBRUARY 1976

1. Report No.	2. Government Accession No.	3. Recipient's Catalog No.
NASA TN D-8142		

4. Title and Subtitle
AN ANALYTICAL STUDY OF TURBULENCE RESPONSES, INCLUDING HORIZONTAL-TAIL LOADS, OF A CONTROL-CONFIGURED VEHICLE WITH RELAXED STATIC STABILITY

5. Report Date: February 1976

6. Performing Organization Code:

7. Author(s)
Boyd Perry III

8. Performing Organization Report No.: L-10389

9. Performing Organization Name and Address
NASA Langley Research Center
Hampton, Va. 23665

10. Work Unit No.: 505-02-21-03

11. Contract or Grant No.:

12. Sponsoring Agency Name and Address
National Aeronautics and Space Administration
Washington, D.C. 20546

13. Type of Report and Period Covered: Technical Note

14. Sponsoring Agency Code:

15. Supplementary Notes
Part of the information presented in this report was included in a thesis entitled "An Analytical Study of Turbulence Responses, Including Horizontal-Tail Loads, of a Control-Configured Jet Transport With Relaxed Static Stability" submitted to The George Washington University in partial fulfillment of the requirements for the degree of Master of Science, February 1975.

16. Abstract

A static stability augmentation system (SSAS) with angle-of-attack, pitch-rate, and forward-speed feedback is used to stabilize control-configured rigid vehicles with relaxed static stability. Airplane configurations include a baseline (statically stable) configuration and two representative control-configured vehicle (statically unstable) configurations. The first statically unstable configuration has baseline geometry and an aft center of gravity; the second statically unstable configuration has reduced tail length and area and a forward neutral point. Stability, flying-qualities, and maneuverability requirements are imposed on the airplane-SSAS systems. Turbulence responses of the rigid airframe and tail loads are examined in terms of configuration changes for a given control law and in terms of control law changes for a given configuration.

17. Key Words (Suggested by Author(s))
Atmospheric turbulence
Control-configured vehicle
Relaxed static stability
Airplane response
Tail loads

18. Distribution Statement
Unclassified – Unlimited

Subject Category 08

19. Security Classif. (of this report)	20. Security Classif. (of this page)	21. No. of Pages	22. Price*
Unclassified	Unclassified	61	$4.25

*For sale by the National Technical Information Service, Springfield, Virginia 22161

AN ANALYTICAL STUDY OF TURBULENCE RESPONSES, INCLUDING HORIZONTAL-TAIL LOADS, OF A CONTROL-CONFIGURED VEHICLE WITH RELAXED STATIC STABILITY*

Boyd Perry III
Langley Research Center

SUMMARY

A static stability augmentation system (SSAS) with angle-of-attack, pitch-rate, and forward-speed feedback is used to stabilize control-configured rigid vehicles with relaxed static stability. Airplane configurations include a baseline (statically stable) configuration and two representative control-configured vehicle (statically unstable) configurations. The first statically unstable configuration has baseline geometry and an aft center of gravity; the second statically unstable configuration has reduced tail length and area and a forward neutral point. Stability, flying-qualities, and maneuverability requirements are imposed on the airplane-SSAS systems. Turbulence responses of the rigid airframe and tail loads are examined in terms of configuration changes for a given control law and in terms of control law changes for a given configuration. Results indicate that even though the tail loads for the unstable configuration with the small tail are less than those for the stable configuration, the tail-load intensity is larger.

INTRODUCTION

Analytical studies of turbulence responses of autopilot-controlled vehicles that have been reported in the open literature include parametric variations in feedback gains (refs. 1 and 2), airplane geometry and flight conditions (ref. 2), and Mach number (ref. 3). In each study, the autopilots maintained the example airplanes on prescribed flight paths and the example airplanes were inherently longitudinally statically stable at the flight conditions investigated. In an earlier study (ref. 4) the elastic- and rigid-body turbulence responses of a long-range bomber airplane were calculated for a number of stability augmentation systems. Again, the airplane was inherently longitudinally statically stable.

*Part of the information presented in this report was included in a thesis entitled "An Analytical Study of Turbulence Responses, Including Horizontal-Tail Loads, of a Control-Configured Jet Transport With Relaxed Static Stability" submitted to The George Washington University in partial fulfillment of the requirements for the degree of Master of Science, February 1975.

The recent emergence of the control-configured vehicle (CCV) concept has introduced airplanes which are deliberately designed to be longitudinally statically unstable (referred to as relaxed static stability) at certain flight conditions within their flight envelopes. (See refs. 5 to 10.) These vehicles rely on static stability augmentation systems (SSAS) for longitudinal static stability augmentation at all times when the vehicle is in flight. (See refs. 9 to 11.) Because the CCV concept is new, there are some technical areas which have received little attention in the open literature. One such area is the study of control-configured vehicles with relaxed static stability flying through continuous atmospheric turbulence.

The purpose of this paper is to determine airframe and horizontal-tail-load turbulence responses of a control-configured rigid vehicle with relaxed static stability (RSS). The vehicle is representative of small executive jet transports. Three variations of the same airplane configuration are investigated at two different flight conditions. The three airplane configurations include a baseline (longitudinally statically stable) conventional configuration and two configurations with relaxed static stability (one with an altered center of gravity and one with reduced tail length and area). The configurations with RSS are artificially stabilized with a static stability augmentation system which features angle-of-attack feedback, pitch-rate feedback, and forward-speed feedback to the elevator. The flight conditions are Mach numbers of 0.50 and 0.75 at an altitude of 6100 meters. Random process theory is used to determine the rigid-airframe and tail-load turbulence responses. Only the vertical component of turbulence is considered. The turbulence varies in the direction of flight but does not vary along the span (one-dimensional gust field) and it is represented by the Von Karman power spectrum. The rigid-airframe responses include the longitudinal degrees of freedom and other derived quantities; and the tail-load responses include torque and bending moment of the horizontal tail. Stability requirements, flying-qualities requirements, and maneuverability requirements are imposed on the SSAS in each configuration with RSS. These requirements are first satisfied by appropriate feedback gain selections and then the turbulence responses of each configuration with RSS are calculated and compared with the turbulence responses of the baseline configuration. In addition to the analysis and discussion of the turbulence responses given in the paper, two appendixes are presented: Appendix A defines flying-qualities criteria in the complex plane; appendix B defines the apparent maneuverability for the augmented airplane and examines the effect of the feedback gains on the apparent maneuverability.

SYMBOLS

$A(s)$ aerodynamic coefficient matrix

$\overline{A}_R$ ratio of root-mean-square value of response R to root-mean-square value of gust input

b	wing span, m
b_t	horizontal-tail span, m
C_{ij}	tail-load coefficients (see eqs. (8) and (9))
C_L	lift coefficient
$C_{L,o}$	lift coefficient for steady flight condition
$C_{M,b}$	bending-moment coefficient, $\frac{M_b}{\frac{1}{2}\rho u_o^2 S_t \bar{c}_t}$
C_m	pitching-moment coefficient
C'_{m_q}	apparent C_{m_q} stability derivative
C'_{m_α}	apparent C_{m_α} stability derivative
C_T	torque coefficient, $\frac{T}{\frac{1}{2}\rho u_o^2 S_t \bar{c}_t}$
C_x	x-force coefficient
C_z	z-force coefficient
C'_{z_q}	apparent C_{z_q} stability derivative
C'_{z_α}	apparent C_{z_α} stability derivative
$\bar{c}$	wing mean aerodynamic chord, m
c_t	local chord of horizontal tail, m
$\bar{c}_t$	horizontal-tail mean aerodynamic chord, m
$f(s)$	vertical-gust column matrix
g	acceleration due to gravity

H_R	frequency-response function of response R
h	center-of-gravity position in terms of $\bar{c}$
h_m	stick-fixed maneuver point in terms of $\bar{c}$
h'_m	apparent stick-fixed maneuver point in terms of $\bar{c}$
h_n	stick-fixed neutral point in terms of $\bar{c}$
h'_n	apparent stick-fixed neutral point in terms of $\bar{c}$
I_{YY}	airplane pitch moment of inertia, kg-m^2
i_B	nondimensional pitch moment of inertia, $8I_{YY}/\rho S\bar{c}^3$
K_u	forward-speed feedback gain, rad/m/sec
K_α	angle-of-attack feedback gain, rad/rad
K_δ	gear ratio, rad/rad
$K_{\dot{\theta}}$	pitch-rate feedback gain, rad/rad/sec
k_n	undamped natural reduced frequency, $\omega_n\bar{c}/2u_o$
k_o	damped natural reduced frequency, $\omega_o\bar{c}/2u_o$
L	scale of turbulence, m
ℓ_t	distance from center of gravity to horizontal-tail aerodynamic center, m
M	moment about Y-axis; also Mach number
M_b	horizontal-tail bending moment outboard of 24 percent semispan, N-m
m	mass of airplane, kg
n	acceleration factor, g units

Δn	vertical acceleration of airplane center of gravity in g units, positive down
q	column matrix of independent variables
R	general turbulence response ($\hat{u}$, Δn, $M_{\dot{b}}$, etc.)
S	wing area, m^2
S_t	horizontal-tail area, m^2
s	Laplace variable
T	horizontal-tail torque about 40 percent chord, N-m
t^*	airplane characteristic time, $\bar{c}/2u_o$
t_1	elevator servo characteristic time, sec
u	forward-speed perturbation, m/sec
$\hat{u}$	nondimensional forward-speed perturbation, u/u_o
u_o	airplane forward speed, m/sec
w	perturbation velocity in z-direction, positive down, m/sec
w_g	vertical-gust velocity, positive up, m/sec
X	force in x-direction
Z	force in z-direction
α	airplane angle-of-attack perturbation, w/u_o
α_g	gust angle of attack, $-w_g/u_o$
α_t	horizontal-tail angle of attack
δ	elevator deflection perturbation, positive trailing edge down, rad
$\Delta\delta$	elevator deflection necessary to hold a pull-up maneuver of load factor n, rad

$\Delta\delta'$ apparent elevator deflection necessary to initiate a pull-up maneuver of load factor n, rad

$\Delta\delta_s$ control-stick deflection, rad

ϵ downwash angle at horizontal tail, rad

ζ damping ratio

θ pitch-angle perturbation, positive nose up

Λ_t sweep angle of horizontal-tail 40 percent chord, deg

$\Lambda_{.25}$ sweep angle of wing quarter chord, deg

μ nondimensional airplane mass, $2m/\rho S\bar{c}$

ρ air density, kg/m^3

σ real part of complex number

σ_R root-mean-square value of response R

σ_{w_g} root-mean-square value of vertical-gust velocity, m/sec

τ transport time lag, ℓ_t/u_o

$\Phi_{w_g}(\omega)$ power spectral density function of vertical-gust velocity, $(m/sec)^2/rad/sec$

ω circular frequency, rad/sec

ω_n undamped natural circular frequency, rad/sec

ω_o damped natural circular frequency, $\omega_n\sqrt{1 - \zeta^2}$, rad/sec

$$C_{x_u} = \frac{\partial C_x}{\partial \hat{u}} \qquad C_{m_u} = \frac{\partial C_m}{\partial \hat{u}}$$

$$C_{x_\alpha} = \frac{\partial C_x}{\partial \alpha} \qquad C_{m_\alpha} = \frac{\partial C_m}{\partial \alpha}$$

$$C_{z_u} = \frac{\partial C_z}{\partial \hat{u}}$$

$$C_{z_\alpha} = \frac{\partial C_z}{\partial \alpha}$$

$$C_{z_{\dot{\alpha}}} = \frac{\partial C_z}{\partial \left(\frac{\dot{\alpha}\bar{c}}{2u_o}\right)}$$

$$C_{z_q} = \frac{\partial C_z}{\partial \left(\frac{q\bar{c}}{2u_o}\right)}$$

$$C_{z_\delta} = \frac{\partial C_z}{\partial \delta}$$

$$C_{m_{\dot{\alpha}}} = \frac{\partial C_m}{\partial \left(\frac{\dot{\alpha}\bar{c}}{2u_o}\right)}$$

$$C_{m_q} = \frac{\partial C_m}{\partial \left(\frac{q\bar{c}}{2u_o}\right)}$$

$$C_{m_\delta} = \frac{\partial C_m}{\partial \delta}$$

$$C_{L_\alpha} = \frac{\partial C_L}{\partial \alpha}$$

Subscripts:

M_b	bending moment
sp	short period
T	torque
t	horizontal tail
u	forward speed
$\hat{u}$	forward speed (nondimensional)
α	angle of attack
α_t	horizontal-tail angle of attack
Δn	center-of-gravity vertical acceleration

δ elevator deflection

θ pitch angle

$\dot{\theta}$ pitch rate

Abbreviations:

CCV control-configured vehicle

FQC flying-qualities criteria

RSS relaxed static stability

rms root mean square

SSAS static stability augmentation system

A dot over a quantity represents the derivative of that quantity with respect to time.

ANALYSIS

Equations of Motion

The equations of motion used in this study are the three degree-of-freedom, longitudinal, small-perturbation equations (ref. 12), and an equation which describes the behavior of the static stability augmentation system. The equations of motion are written in the stability axes system and are presented in equation (1).

$$\begin{bmatrix} 2\mu t^*s - C_{x_u} & -C_{x_\alpha} & C_{L_o} & 0 \\ 2C_{L_o} - C_{z_u} & 2\mu t^*s - C_{z_\alpha} - C_{z_{\dot{\alpha}}} t^*s \left[\frac{1 - e^{-\tau s}}{\tau s}\right] & \left(-2\mu - C_{z_q}\right) t^*s & -C_{z_\delta} \\ -C_{m_u} & -C_{m_\alpha} - C_{m_{\dot{\alpha}}} t^*s \left[\frac{1 - e^{-\tau s}}{\tau s}\right] & \iota_B t^{*2} s^2 - C_{m_q} t^*s & -C_{m_\delta} \\ -\frac{K_u u_o}{1 + t_1 s} & -\frac{K_\alpha}{1 + t_1 s} & -\frac{K_{\dot{\theta}} s}{1 + t_1 s} & 1 \end{bmatrix} \begin{Bmatrix} \hat{u} \\ \alpha \\ \theta \\ \delta \end{Bmatrix} = \alpha_g \begin{Bmatrix} C_{x_\alpha} \\ C_{z_\alpha} + \left(C_{z_{\dot{\alpha}}} - C_{z_q}\right) t^*s \left[\frac{1 - e^{-\tau s}}{\tau s}\right] \\ C_{m_\alpha} + \left(C_{m_{\dot{\alpha}}} - C_{m_q}\right) t^*s \left[\frac{1 - e^{-\tau s}}{\tau s}\right] \\ \frac{K_\alpha}{1 + t_1 s} \end{Bmatrix} \tag{1}$$

The stability derivatives are defined in the list of symbols; t^* is the airplane characteristic time defined in the list of symbols; t_1 is the servo-actuator characteristic time discussed below; τ is the transport time discussed below; μ and i_B are nondimensional airplane mass and pitch moment of inertia, respectively; K_u, K_α, and $K_{\dot{\theta}}$ are feedback gains; $\hat{u}$, α, θ, and δ are the small-perturbation independent variables; α_g is the gust angle of attack; and s is the Laplace variable.

Equation (1) contains terms which account for the transport lags in downwash from wing to tail and the transport lag in gust encounter from wing to tail. These terms are indicated by the rectangular boxes in equation (1) and they reduce to unity if the first two terms of power series representation are substituted for the exponential (ref. 12). The time τ in these terms is the time required for the airplane to traverse a distance equal to that between its center of gravity and the aerodynamic center of its horizontal tail. The power series representation was used to calculate the roots of the characteristic equation (for example, in root locus studies). The exponential was used to calculate the turbulence responses from the power spectral density functions.

The last row of equation (1) describes the elevator deflection for the static stability augmentation system and may be expressed as

$$\delta = \frac{1}{1 + t_1 s}\left[K_u\left(u_o\hat{u}\right) + K_\alpha\left(\alpha + \alpha_g\right) + K_{\dot{\theta}}(s\theta)\right] \tag{2}$$

Equation (2) states that the elevator is commanded to deflect in proportion to $\hat{u}$, α, α_g, and $\dot{\theta}$ and it is assumed that sensors are available to measure u, $\alpha + \alpha_g$, and $\dot{\theta}$ directly. It is also assumed that the α-sensor is located at the airplane center of gravity. (Other locations will produce changes in the stability characteristics and in the turbulence responses. For example, if the α-sensor is located at the nose of the airplane, a degree of gust anticipation is introduced relative to the present system. This anticipation may compensate, to a certain extent, for the lag in the servo actuator. The nose location will also cause the α-sensor to respond to pitching; thus, changes in K_α will produce changes in an effective $K_{\dot{\theta}}$.) The quantity $\frac{1}{1 + t_1 s}$ in equation (2) represents the dynamics of the servo actuator and has one-minus-exponential type response to a step input. For such a response, t_1 is the time it takes the elevator to sweep through approximately two-thirds of its final deflection. In this study, $t_1 = 0.066$ sec (less than 1/10 sec as recommended in ref. 13), and consequently very much less than the period of the short-period mode. Equation (2) represents an idealized situation in that elevator aerodynamic hinge moments do not affect the response of the elevator.

The airframe frequency-response functions describe the responses of the airplane to a unit sinusoidal one-dimensional gust field of varying frequencies. Equation (1) may be written as

$$\left[A(s)\right]\left\{q(s)\right\} = \alpha_g\left\{f(s)\right\} \tag{3}$$

The frequency-response functions are obtained by solving equation (3) for the independent variables and substituting $i\omega$ for s. When $-w_g/u_o$ is substituted for α_g, the solution of equation (3) is

$$\left\{q(i\omega)\right\} = w_g\left\{H(i\omega)\right\} \tag{4}$$

where

$$\left\{H(i\omega)\right\} = \begin{Bmatrix} H_{\frac{\hat{u}}{w_g}}(i\omega) \\ H_{\frac{\alpha}{w_g}}(i\omega) \\ H_{\frac{\theta}{w_g}}(i\omega) \\ H_{\frac{\delta}{w_g}}(i\omega) \end{Bmatrix} = -\frac{1}{u_o}\left[A(i\omega)\right]^{-1}\left\{f(i\omega)\right\} \tag{5}$$

Equation (5) is the matrix of frequency-response functions in per-unit-gust-velocity form. The frequency-response functions of center-of-gravity vertical acceleration and horizontal-tail total angle of attack are expressed in terms of the frequency-response functions of the independent variables as

$$H_{\frac{\Delta n}{w_g}}(i\omega) = i\omega\frac{u_o}{g}\left[H_{\frac{\alpha}{w_g}}(i\omega) - H_{\frac{\theta}{w_g}}(i\omega)\right] \tag{6}$$

$$H_{\frac{\alpha_t}{w_g}}(i\omega) = \left(1 - e^{-i\omega\tau}\frac{\partial\epsilon}{\partial\alpha}\right)H_{\frac{\alpha}{w_g}}(i\omega) + i\omega\frac{\ell_t}{u_o}H_{\frac{\theta}{w_g}}(i\omega) - \frac{1}{u_o}\left(1 - \frac{\partial\epsilon}{\partial\alpha}\right)e^{-i\omega\tau} \tag{7}$$

Tail-Load Equations

The tail-load geometry is illustrated in sketch (a).

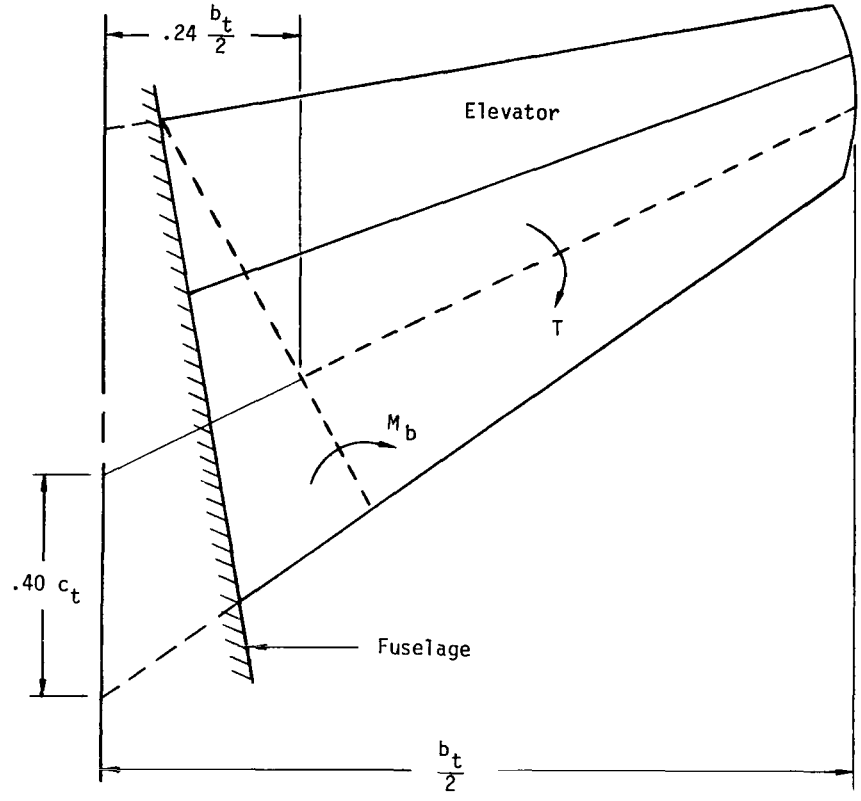

Sketch (a)

The horizontal tail is swept and tapered with a full-span elevator and a frictionless hinge. The quantities T and M_b are the torque and bending moment calculated about the two perpendicular axes indicated by the dashed lines. The torque axis is the 40-percent chord line. The bending-moment axis intersects the torque axis at the 24-percent semispan position. Torque and bending moment are calculated about their respective axes by summation of the forces acting outboard of the bending-moment axis.

Both torque and bending moment contain components due to aerodynamic and inertia forces. The aerodynamic components result from the motion of the vehicle, the atmospheric turbulence, and the deflection of the elevator and they are obtained by integrating the aerodynamic-force distributions over the tail surface. The inertia components result from the vertical plunging and pitching accelerations at the tail and they are obtained by integrating the mass distribution of the tail over the tail surface and multiplying the result by the acceleration at the tail.

The following tail-load equations are derived in a manner similar to that described in appendix B of reference 1:

$$T = C_{11}\alpha_t + C_{12}\delta + C_{13}\,\Delta n + C_{14}\ddot{\theta} \tag{8}$$

$$B = C_{21}\alpha_t + C_{22}\delta + C_{23}\,\Delta n + C_{24}\ddot{\theta} \tag{9}$$

where α_t is the horizontal-tail total angle of attack, δ is the elevator deflection angle, Δn is the vertical acceleration at the airplane center of gravity in g units, and $\ddot{\theta}$ is the pitching acceleration. The C_{ij} coefficients are constants obtained from the integration of the aerodynamic and mass distributions. Coefficients C_{i1} and C_{i2} are coefficients of the aerodynamic terms, and coefficients C_{i3} and C_{i4} are coefficients of the inertia terms.

Torque and bending moment are expressed as dimensionless tail-load coefficients by dividing equations (8) and (9) by the quantity $\frac{1}{2}\rho u_o^2 S_t \bar{c}_t$

$$C_T = \frac{T}{\frac{1}{2}\rho u_o^2 S_t \bar{c}_t} \tag{10}$$

$$C_{M,b} = \frac{M_b}{\frac{1}{2}\rho u_o^2 S_t \bar{c}_t} \tag{11}$$

Because the quantity $\frac{1}{2}\rho u_o^2 S_t \bar{c}_t$ is proportional to the volume of the horizontal tail, equations (10) and (11) are measures of the horizontal-tail loading intensity (tail loads per tail volume). Equations (10) and (11) are useful because they permit comparisons of tail loads on tails of different sizes.

Frequency-response functions of the torque and bending moment of the horizontal tail are expressed in terms of the frequency-response functions of the independent variables and equations (6) and (7) as

$$H_{\frac{T}{w_g}}(i\omega) = C_{11}H_{\frac{\alpha_t}{w_g}}(i\omega) + C_{12}H_{\frac{\delta}{w_g}}(i\omega) + C_{13}H_{\frac{\Delta n}{w_g}}(i\omega) - C_{14}\omega^2 H_{\frac{\theta}{w_g}}(i\omega) \tag{12}$$

$$H_{\frac{M,b}{w_g}}(i\omega) = C_{21}H_{\frac{\alpha_t}{w_g}}(i\omega) + C_{22}H_{\frac{\delta}{w_g}}(i\omega) + C_{23}H_{\frac{\Delta n}{w_g}}(i\omega) - C_{24}\omega^2 H_{\frac{\theta}{w_g}}(i\omega) \tag{13}$$

Frequency-response functions of the torque and bending-moment coefficients are expressed in terms of equations (12) and (13) as

$$H_{C_{\frac{T}{w_g}}}(i\omega) = \frac{H_{\frac{T}{w_g}}(i\omega)}{\frac{1}{2}\rho u_o^2 S_t \bar{c}_t} \tag{14}$$

$$H_{C_{\frac{M,b}{w_g}}}(i\omega) = \frac{H_{\frac{M,b}{w_g}}(i\omega)}{\frac{1}{2}\rho u_o^2 S_t \bar{c}_t} \tag{15}$$

Statistical Representations

The airplane is treated as a linear system and its responses to random atmospheric turbulence are determined in a statistical sense by use of random process theory. In random process theory the power spectral density function (power spectrum) contains all the required statistical information describing a Gaussian random process with zero mean.

Atmospheric turbulence.- The Von Karman power spectrum (ref. 14) was chosen to describe the vertical component of one-dimensional atmospheric turbulence

$$\Phi_{w_g}(\omega) = \frac{\sigma_{w_g}^2 L}{\pi u_o} \frac{1 + \frac{8}{3}\left(1.339 \frac{L}{u_o}\omega\right)^2}{\left[1 + \left(1.339 \frac{L}{u_o}\omega\right)^2\right]^{11/6}} \tag{16}$$

The quantity ω is the circular frequency in radians per second; u_o is the forward speed of the example airplane; L is the scale of turbulence, chosen to be 762 m; and σ_{w_g} is the root-mean-square (rms) value of the vertical-gust velocity, assigned to be 1 m/sec. The Von Karman power spectrum approaches a constant value at the low circular frequencies and is characterized by a -5/3 power law at the high circular frequencies.

Airplane responses.- The root-mean-square values of the airplane responses are the quantities of interest in this paper. The rms value of a general response (normalized to the unit rms vertical-gust velocity) is calculated in the following manner:

$$\frac{\sigma_R}{\sigma_{w_g}} = \left[\frac{\int_0^\infty \left| H_R(i\omega) \right|^2 \Phi_{w_g}(\omega)\, d\omega}{\sigma^2_{w_g}} \right]^{1/2} \tag{17}$$

where $H_R(i\omega)$ is the frequency-response function of a general response R, and $\Phi_{w_g}(\omega)$ is the Von Karman power spectrum of equation (16). In actual practice the upper limits of integration in equation (17) were between 100 and 200 rad/sec. As stated in the discussion of the equations of motion, the full exponentials (within the boxes in eq. (1)) were retained in evaluating the integral in equation (17). Had the first two terms of the power series representation been used instead of the full exponential, the integral in equation (17) would not have converged. Equation (17), when used in conjunction with the frequency-response functions of equations (5) to (7) and (12) to (15), yields the rms values of the turbulence responses. For the remainder of this paper, the ratio σ_R/σ_{w_g} will be replaced by the symbol $\overline{A}_R$.

STATIC STABILITY AUGMENTATION SYSTEM

The static stability augmentation system (SSAS) provides stability and adds damping to those configurations with relaxed static stability. The SSAS contains three feedback loops: an angle-of-attack loop, a pitch-rate loop, and a forward-speed loop, all of which act through the elevator. Each feedback loop has a corresponding feedback gain. Reference 7 states that such feedback to a pitching-moment control surface is adequate to provide stability to airplanes with relaxed static stability. A block diagram showing the airframe dynamics, the SSAS feedback signals, and the atmospheric turbulence is shown in figure 1.

SSAS Requirements

Various requirements are imposed on the static stability augmentation system such as providing stability, satisfying flying-qualities criteria, and increasing maneuverability. These requirements are met by varying the SSAS feedback gains.

Stability exists when all roots of a system characteristic equation lie in the left half of the complex plane. For the configurations with relaxed static stability, the originally statically unstable mode is stabilized by varying the SSAS gains until all roots are in the left half plane. The presence of the servo-dynamics transfer function in figure 1 results in an additional root in the system characteristic equation. This root (referred to as the servo root) is real and it must also lie in the left half plane for stability.

Flying qualities criteria (FQC) are those for level 1 as defined in reference 15 in terms of phugoid and short-period damping ratios and undamped natural frequencies. These FQC may be visualized as regions in the complex plane (referred to here as FQC regions) within which the phugoid and short-period roots lie (ref. 16). The FQC are satisfied by varying the SSAS gains until the phugoid and short-period roots lie within their respective FQC regions. Figure 2 shows the phugoid and short-period FQC regions in the complex plane. Appendix A contains the derivation of the form of the FQC regions as shown in figure 2. Because of symmetry about the real axis, only the portions of the FQC regions in the second quadrant are presented. The insets show the values of undamped natural frequencies and damping ratios which define each region. The fan shape of the short-period region indicates that short-period FQC are specified in terms of both frequency and damping. The shape of the phugoid region indicates that phugoid FQC are specified in terms of damping only. Because the FQC regions lie totally within the left half of the complex plane, stability exists whenever the FQC are satisfied.

Defining flying-qualities criteria is complicated by the presence of the servo root. The phugoid and short-period flying qualities are determined by the locations of the phugoid and short-period roots in the complex plane. If the servo root is not "close" to either the phugoid pair or the short-period pair of roots, it will not seriously affect the physical interpretation of those roots. However, if the servo root is close to either pair, it will cause coupled motion between a conventional mode and the servo mode; and the FQC are not defined for such motion.

Maneuverability in the longitudinal degrees of freedom usually is defined by the elevator angle per g, which is the elevator deflection required to trim the airplane in steady accelerated flight (such as a steady pull-up maneuver) of constant load factor. This deflection is related to the control-stick deflection through the gear ratio. For configurations with relaxed static stability, the SSAS provides a portion of the required elevator deflection in steady accelerated flight. In such configurations an apparent maneuverability is defined in terms of the control-stick deflection. The control-stick deflection corresponds to an apparent elevator deflection (through the gear ratio) which the pilot commands in conjunction with the SSAS to achieve the steady pull-up maneuver. This concept is mathematically described in terms of stability derivatives and SSAS feedback gains in appendix B. For the present study, the maneuverability requirement for configurations with relaxed static stability is that the apparent elevator angle per g is 25 percent less than the baseline elevator angle per g.

Control Laws

The static stability augmentation system is configured to perform two alternate functions: (1) to match the flying qualities of the baseline short-period mode without

regard for changes in maneuverability, or (2) to satisfy the maneuverability requirement and still maintain satisfactory flying qualities as defined by figure 2. Certain combinations of feedback gains are chosen to perform each of these two functions and such combinations of gains will be referred to as control laws. One control law to perform function 1 and two control laws to perform function 2 are discussed below.

Control law 1 uses K_α and $K_{\dot{\theta}}$ feedback gains to perform function 1 and unique combinations of these gains are found to exist. Because the short-period mode is insensitive to changes in the K_u feedback gain, K_u is set to zero.

Control law 2 uses K_α and $K_{\dot{\theta}}$ feedback gains (K_u set to zero) to perform function 2. Unique combinations of these gains do not exist but single pairs of gains are selected in the following manner: the smallest K_α is chosen to satisfy the FQC and then $K_{\dot{\theta}}$ is adjusted until the maneuverability condition is satisfied.

Control law 3 uses K_u and $K_{\dot{\theta}}$ feedback gains (K_α set to zero) to perform function 2. Unique combinations of these gains do not exist either but single pairs of gains are selected in the following manner: $K_{\dot{\theta}}$ is chosen to satisfy the maneuverability condition and then the smallest K_u is chosen to satisfy the FQC.

AIRPLANE CONFIGURATIONS AND FLIGHT CONDITIONS

Three airplane configurations are examined in this study: one with inherent static stability and two with relaxed static stability (RSS). The configurations are intended to represent one conventional design and two possible CCV-type designs of the executive-jet-transport class of airplanes. The conventional, or baseline, configuration has nominal weight and geometry and a positive static margin. Both configurations with RSS, through either weight redistributions or geometry alterations, have negative static margins at the flight conditions investigated. The first of these has the same geometry and weight as the baseline configuration, but a negative static margin due to an aft center-of-gravity position. The second configuration with RSS has altered geometry and reduced weight: the tail area is reduced 50 percent and the tail length is reduced 10 percent; thus there is a 5-percent reduction in total airplane weight. In this case the negative static margin is due to a forward-neutral point. Figure 3 shows the relative sizes of the wing and tail and the relative locations of the center of gravity and neutral point for each configuration. Table I presents pertinent physical dimensions for each configuration. References 8, 10, and 11 indicate that the geometry alterations and weight reductions pertaining to the second configuration with RSS are possible for a control-configured transport aircraft.

The tails of the configurations with RSS are assumed to have enough authority to satisfy control-moment requirements such as nose wheel unstick. Performing detailed tail-sizing and weight-distribution studies is beyond the scope of this paper, but such

studies must be performed when designing an actual aircraft. For simplicity, when referring to either of the two configurations with RSS, they will be identified by their geometry and static stability characteristics: nominal unstable for the first and reduced unstable for the second.

The flight conditions investigated are Mach numbers of 0.50 and 0.75 at an altitude of 6100 m. Table II contains center-of-gravity position and stability parameters for all configurations at both flight conditions. Table III contains the stability derivatives for all configurations at both flight conditions.

RESULTS AND DISCUSSION

This section of the paper contains four parts: the first three examine the dynamic characteristics (including stability, flying qualities, and maneuverability) and turbulence responses for each control law; and the fourth examines the turbulence responses for a given control law in terms of configuration changes and the turbulence responses for a given configuration in terms of control-law changes.

Control Law 1

Control law 1 uses angle-of-attack and pitch-rate feedback to match the flying qualities (that is, frequency and damping) of the baseline short-period mode without regard for changes in maneuverability. Angle-of-attack feedback provides stability to the RSS configurations and pitch-rate feedback provides additional damping.

Dynamic characteristics.- Table IV contains the values of the K_α and $K_{\dot{\theta}}$ feedback gains for control law 1, the values of the natural frequencies and damping ratios of the phugoid and short-period modes, and the values of the apparent elevator angles per g. Table IV confirms that the flying qualities of the baseline short-period mode are matched; at both Mach numbers the short-period natural frequencies and damping ratios of the RSS configurations match those of the baseline configuration almost identically. It also indicates that larger amounts of K_α and $K_{\dot{\theta}}$ are required for the reduced-unstable configuration than for the nominal-unstable configuration because the smaller tail of the reduced-unstable configuration results in less elevator effectiveness. Smaller amounts of K_α and $K_{\dot{\theta}}$ are required at the higher Mach number because aerodynamic forces are greater for a given elevator deflection. The last column in table IV contains the apparent elevator angle per g for each configuration and flight condition. The apparent elevator angle per g for the nominal-unstable configuration is within 2 percent of the value of the actual elevator angle per g for the baseline configuration. The apparent elevator angle per g for the reduced-unstable configuration is (within 4 percent) twice that of the baseline configuration, and reflects the 50-percent reduction in tail area.

Figure 4 shows the phugoid and short-period roots (corresponding to the phugoid and short-period parameters of table IV) plotted in the complex plane. The cluster of short-period roots for each Mach number indicates that the frequency and damping of the baseline short-period mode have been matched. Both the phugoid and short-period roots are within their respective FQC regions.

Figure 5 contains a typical root locus of the characteristic equation for changes in K_α and $K_{\dot{\theta}}$. The reduced-unstable configuration at Mach number 0.50 was chosen for the example; however, the other configurations show the same trends. The solid lines represent increases in K_α $\left(\text{with } K_{\dot{\theta}} = 0\right)$ and the dashed lines represent increases in $K_{\dot{\theta}}$ $\left(\text{with } K_\alpha = 0.88\right)$. Figure 5(b) is an enlarged view of the area near the origin in figure 5(a). When both gains are zero, the airplane is statically unstable and the roots of the characteristic equation are indicated by x. As K_α increases, the dead-beat (non-oscillatory) unstable root crosses into the left half plane and combines with one of the roots from the classical third mode (ref. 14) to form the augmented phugoid mode. The other root from the third mode combines with another originally dead beat but stable root to form the augmented short-period mode. With K_α set at 0.88, $K_{\dot{\theta}}$ is increased until the frequency and damping of the augmented short-period mode match those of the baseline short-period mode. There is an additional dead-beat root associated with the elevator servo transfer function. The root is stable and it is located far to the left beyond the part of the real axis shown in figure 5(a). Its characteristic motion is primarily in pitch with a time to half amplitude of 0.049 sec, only slightly slower than the zero-gain time to half amplitude of 0.046 sec.

Turbulence responses.- Table V contains the turbulence responses (the $\overline{A}$'s) for all configurations and flight conditions for control law 1, and the subscripts on the $\overline{A}$'s indicate the appropriate response. When examining some of the turbulence responses of the baseline configuration at both Mach numbers, it was observed that: (1) the angle of attack $\overline{A}_\alpha$ varied inversely with Mach number; (2) the vertical component of center-of-gravity acceleration $\overline{A}_{\Delta n}$ increases with Mach number, which reflects the corresponding increases in forward speed and airplane lift-curve slope; and (3) both horizontal-tail torque and bending moment, $\overline{A}_T$ and $\overline{A}_{M,b}$, increase with Mach number and reflect the increases in the aerodynamic and inertia components of both.

An examination of the turbulence responses from configuration to configuration at a given Mach number revealed that the angle-of-attack response remains practically unchanged at each Mach number. Angle of attack is primarily a short-period phenomenon. Because short-period flying qualities are matched almost exactly and because α-feedback predominates over $\dot{\theta}$-feedback, $\overline{A}_\alpha$ remains unchanged. The pitch angle $\overline{A}_\theta$ is smaller for configurations with relaxed static stability for both Mach numbers (reductions ranging from 20 percent to 45 percent). However, center-of-gravity vertical acceleration $\overline{A}_{\Delta n}$

increases between 10 percent and 15 percent in these configurations, probably as a result of the decrease in $\overline{A}_\theta$. Elevator deflection $\overline{A}_\delta$ increases from the nominal-unstable to the reduced-unstable configuration because of the increased feedback gains for the reduced-unstable configuration. Horizontal-tail torque and bending moment are larger for the nominal-unstable configuration than for the baseline configuration but smaller for the reduced-unstable configuration. The larger $\overline{A}$ values for the nominal-unstable configuration are primarily a result of the increase in the aerodynamic components from elevator deflection. Even though the tail loads are reduced (torque over 60 percent; bending moment over 15 percent) in the reduced-unstable configuration, the horizontal-tail loading intensity (as indicated by the tail-load coefficients) is still larger at both Mach numbers.

Inspection of the components of torque and bending moment revealed that approximately 90 percent of each is due to aerodynamic contributions and that the remaining 10 percent is due to the inertia contributions. Although the total aerodynamic forces on the tail due to α_t and δ are of the same order of magnitude, the net contribution to torque from elevator deflection is small compared with the net contribution from tail angle of attack. The aerodynamic force distribution due to elevator deflection has approximately equal contributions forward and aft of the 40-percent chord and results in considerable cancellation of torque.

Control Law 2

Control law 2 uses angle-of-attack and pitch-rate feedback to satisfy the maneuverability requirement and at the same time maintain satisfactory flying qualities.

Dynamic characteristics.- Table VI contains the values of K_α and $K_{\dot\theta}$ feedback gains for control law 2, the values of the natural frequencies and damping ratios of the phugoid and short-period modes, and the values of the apparent elevator angles per g. Table VI confirms that the maneuverability requirement (decreasing the apparent elevator angles per g of the RSS configurations 25 percent below the actual elevator angle per g of the baseline configuration) has been satisfied: at both Mach numbers the apparent elevator angles per g are within 1 percent of their required values. Table VI indicates that at both Mach numbers the short-period mode is overdamped (damping ratio greater than unity). It also indicates that larger amounts of K_α are required for the reduced-unstable configuration because its smaller tail results in less elevator effectiveness. Smaller amounts of $K_{\dot\theta}$ are required for the reduced-unstable configuration because the apparent elevator angle per g is a function of both K_α and $K_{\dot\theta}$ (see appendix B) and because the corresponding values of K_α are larger.

Figure 6 shows the phugoid and short-period roots (corresponding to the phugoid and short-period parameters of table VI) plotted in the complex plane. The phugoid and

short-period roots are within their respective FQC regions and thus confirm that the flying-qualities criteria have been satisfied. The overdamped short-period mode of the nominal-unstable configuration appears as two dead-beat roots at each Mach number, with corresponding motion primarily in plunge. Figure 7 contains a typical root locus for changes in K_α and $K_{\dot{\theta}}$ for the reduced-unstable configuration at a Mach number of 0.50. The present root locus initially proceeds in the same manner as the root locus for control law 1 in figure 5. However, in the present root locus, the vertical segment of the short-period mode stops just after entering the FQC region and, as a result, there is a lower damped natural frequency and a higher damping ratio.

Turbulence responses.- Table VII contains the turbulence responses for all configurations and flight conditions for control law 2. When examining the turbulence responses from configuration to configuration at a given Mach number, it was observed that the forward-speed response of the nominal-unstable configuration reflects the increased damping of the phugoid mode. For a Mach number of 0.50, $\overline{A}_{\hat{u}}$ for the nominal-unstable configuration is more than an order of magnitude less than $\overline{A}_{\hat{u}}$ for the baseline configuration. For a Mach number of 0.75, $\overline{A}_{\hat{u}}$ for the nominal-unstable configuration is half an order of magnitude less. The angle of attack is smaller in the configurations with relaxed static stability, and, as was the case for control law 1, $\overline{A}_{\dot{\theta}}$ is also smaller in the configurations with relaxed static stability while $\overline{A}_{\Delta n}$, $\overline{A}_{C_T}$, and $\overline{A}_{C_{M,b}}$ are larger.

When comparing the turbulence responses of control law 2 with those of control law 1, it is observed that while $\overline{A}_{\alpha_t}$, $\overline{A}_{\Delta n}$, $\overline{A}_T$, and $\overline{A}_{C_T}$ increase for control law 2, the remaining turbulence responses decrease. Because angle-of-attack and pitch-rate feedback are present for both sets of results and because the short-period damping is greater for all configurations and Mach numbers for control law 2, the smaller $\overline{A}$ values are the result of the increase in short-period damping. The tail angle of attack increases even though the responses of some of its component parts decrease. The center-of-gravity vertical accelerations for control law 2 are greater than those for control law 1 as a consequence of the corresponding decrease in pitch angle. The torque increased approximately 10 percent in each configuration over the torque for control law 1, but the bending moment decreased approximately 5 percent. Again, at both Mach numbers, the tail loads for the nominal-unstable configuration are significantly larger (at least 20 percent for $\overline{A}_T$; almost 100 percent for $\overline{A}_{M,b}$) than the tail-load responses for the baseline configuration, and the tail-load responses for the reduced-unstable configuration are significantly less (60 percent reductions in $\overline{A}_T$; 25 percent reductions in $\overline{A}_{M,b}$) than the tail-load responses for the baseline configuration. However, as before, the tail-load coefficient responses are significantly larger than the corresponding coefficients in the baseline configuration.

Control Law 3

Control law 3 uses forward-speed and pitch-rate feedback to satisfy the maneuverability requirement and at the same time maintain satisfactory flying qualities.

Dynamic characteristics.- Table VIII contains the values of K_u and $K_{\dot{\theta}}$ feedback gains for control law 3, the values of the natural frequencies and damping ratios of the phugoid and short-period modes, and the values of the apparent elevator angles per g. Table VIII confirms that the maneuverability requirement (decreasing the apparent elevator angle per g of the RSS configurations 25 percent below the actual elevator angle per g of the baseline configuration) has been satisfied: at both Mach numbers the apparent elevator angles per g are within 2 percent of their required values. Table VIII also indicates that larger amounts of K_u and $K_{\dot{\theta}}$ are required for the reduced-unstable configuration because its smaller tail results in less elevator effectiveness, and smaller amounts are required at the higher Mach number because aerodynamic forces are greater for a given elevator deflection.

Figure 8 shows the phugoid and short-period roots (corresponding to the phugoid and short-period parameters of table VIII) plotted in the complex plane. The roots of the phugoid mode for each configuration are very highly damped and are well within the phugoid FQC region. The roots of the short-period mode for each configuration are also well behaved, except that for the nominal-unstable configuration at Mach number 0.50 the short-period FQC are not satisfied. Because of the similarity of the frequencies and damping ratios of the nominal-unstable configurations at the two Mach numbers, it was elected to proceed with the analysis and to calculate the turbulence responses even though the flying-qualities criteria for one of the RSS configurations had not been satisfied.

Figure 9 contains a typical root locus for changes in K_u and $K_{\dot{\theta}}$ for the reduced-unstable configuration at Mach number 0.50. The solid lines for this figure represent increases in K_u $\left(\text{with } K_{\dot{\theta}} = 0.46\right)$ and the dashed lines represent increases in $K_{\dot{\theta}}$ (with $K_u = 0$). When both gains are zero, as with the two previous control laws, the airplane is statically unstable. As $K_{\dot{\theta}}$ increases, three things happen: (1) the dead-beat root at -0.024 in figure 9(a) combines with the servo dead-beat root (which was originally far to the left and out of the figure) to form the augmented short-period mode; (2) the roots of the third mode approach the real axis and split into two dead-beat roots; and (3) the divergent dead-beat root approaches, but does not enter, the left half plane. With $K_{\dot{\theta}}$ constant at 0.46, K_u is increased, as seen in figure 9(b), until the divergent dead-beat root enters the left half plane and combines with a root from the third mode to form the augmented phugoid mode. The short-period roots and the other root from the third mode remain unchanged with increases in K_u. In contrast to control laws 1 and 2 in which variation of K_α only was sufficient to stabilize the configurations with RSS, control law 3 required changes in both K_u and $K_{\dot{\theta}}$ to stabilize such configurations. Also,

unlike control laws 1 and 2 (in which the location of the servo root was well removed from the locations of the phugoid and short-period roots), the servo root for control law 3 is located "between" the phugoid and short-period roots. Such a servo root location, as stated in the section "Analysis," complicates the definition of flying-qualities criteria because of the resulting coupled motion.

Turbulence responses.- Table IX contains the turbulence responses for all configurations and flight conditions for control law 3. When examining the turbulence responses from configuration to configuration at a given Mach number, it is observed that the forward-speed response increases significantly for the configurations with RSS. Angle of attack $\overline{A}_{\alpha}$ for the configurations with RSS decreases on the order of 20 percent with respect to the baseline configuration primarily because of the increase in short-period damping. As with the tail loads calculated for the previous two control laws, the tail loads for the nominal-unstable configuration are larger than those for the baseline configuration, whereas the tail loads for the reduced-unstable configuration are smaller. However, the horizontal-tail loading intensity (as indicated by the tail-load coefficients) is larger than that for the baseline configuration for both RSS configurations and both Mach numbers. When comparing the turbulence responses of control law 3 with those of control law 2, it is observed that the elevator deflection is consistently smaller, and tail angle of attack, center-of-gravity acceleration, and torque are consistently larger. Bending moment is larger for the nominal-unstable configurations but equal or smaller for the reduced-unstable configurations.

Turbulence Response Comparisons

Figure 10 contains bar charts of selected turbulence responses for each control law in terms of configuration changes. The responses presented are the center-of-gravity vertical acceleration, and torque and bending-moment coefficients. The letter designations below each bar chart identify the configuration each response pertains to: B for baseline, NU for nominal unstable, and RU for reduced unstable.

For all control laws and both flight conditions, the center-of-gravity vertical acceleration and both tail-load coefficients are larger for both RSS configurations than for the baseline configuration. With only one exception, the center-of-gravity vertical acceleration and torque coefficient for the nominal-unstable configuration are consistently larger than similar responses for the reduced-unstable configuration for the same control laws and flight conditions. The exceptions occur for control law 3 at a Mach number of 0.50 (fig. 10(c)). With only one exception the bending-moment coefficients for the reduced-unstable configuration are consistently larger than the bending-moment coefficients for the nominal-unstable configuration. The exception occurs for control law 3 at a Mach number of 0.75 (fig. 10(c)). In all cases the bending-moment coefficients for the reduced-

unstable configuration are more than twice as large as the bending-moment coefficients for the baseline configuration for the same control laws and flight conditions.

Figure 11 contains bar charts of selected turbulence responses for both RSS configurations in terms of control law changes. The responses presented are center-of-gravity vertical acceleration, and torque and bending-moment coefficients. The number designations below each bar chart identify the control law that pertains to each response.

For both configurations and both flight conditions, the center-of-gravity vertical acceleration and torque increase with increasing control law designation. The center-of-gravity vertical acceleration increases on the order of 20 percent and the torque increases on the order of 25 percent. This trend indicates that for the gains chosen, increasing maneuverability (control laws 2 and 3) is more costly, at least in terms of acceleration and torque, than matching the flying qualities of the baseline configuration (control law 1). For the nominal-unstable configuration (fig. 11(a)), the bending moment is also largest for control law 3, but the responses are almost identical (within 5 percent) for control laws 1 and 2. For the reduced-unstable configuration (fig. 11(b)), however, the bending moment is largest for control law 1 and has almost identical responses (within 4 percent) for control laws 2 and 3.

CONCLUDING REMARKS

An analytical study has been conducted to determine airframe and horizontal-tail-load turbulence responses of control-configured rigid vehicles with relaxed static stability (RSS). The study included three vehicle configurations: one baseline configuration and two representative control-configured-vehicle configurations with RSS. The configurations with RSS relied on similar static stability augmentation systems (SSAS) for stability and each SSAS featured angle-of-attack (α) feedback, pitch-rate ($\dot{\theta}$) feedback, and forward-speed (u) feedback to the elevator. The flight conditions chosen for the study were Mach numbers 0.50 and 0.75 at an altitude of 6100 m. Three control laws were examined which involved satisfying stability requirements, flying-qualities requirements, and maneuverability requirements by varying the SSAS feedback gains. One control law (using α- and $\dot{\theta}$-feedback) matched the baseline short-period flying qualities exactly with no regard for maneuverability considerations. The other two control laws (one using α- and $\dot{\theta}$-feedback; the other using u- and $\dot{\theta}$-feedback) increased the apparent maneuverability of the RSS configurations over that of the baseline configuration and at the same time satisfied the flying-qualities criteria.

The results of this study indicated that

1. Configurations with relaxed static stability can be stabilized either with angle-of-attack and pitch-rate feedback to the elevator or with forward-speed and pitch-rate feedback to the elevator.

2. For both flight conditions and each control law, the center-of-gravity vertical acceleration and the horizontal-tail-load intensity were larger for either RSS configuration than for the baseline configuration.

3. For both RSS configurations, using the SSAS to increase maneuverability was more costly (on the order of 5 percent) in terms of center-of-gravity vertical acceleration and tail torque, but less costly (on the order of 5 percent) in terms of tail bending moment, than using the SSAS to match the baseline flying qualities.

4. For both RSS configurations, using forward-speed and pitch-rate feedback to increase maneuverability was more costly (on the order of 10 percent) in terms of center-of-gravity vertical acceleration and tail-load intensity than using angle-of-attack and pitch-rate feedback to increase maneuverability.

Langley Research Center
National Aeronautics and Space Administration
Hampton, Va. 23665
January 9, 1976

APPENDIX A

FLYING-QUALITIES CRITERIA

The flying-qualities criteria (FQC) described in reference 15 are defined in terms of upper and lower limits of the stability characteristics (damping ratios and undamped natural frequencies) of the phugoid and short-period modes. The purpose of this appendix is to illustrate an alternate way of presenting the FQC such that they are independent of Mach number.

Damping-ratio and undamped-natural-frequency limits are conveniently represented in the complex plane. Constant damping ratio is represented by a pair of radial lines through the origin of the complex plane and symmetric with respect to the real axis; constant undamped natural frequency is represented by a circle whose center is the origin of the complex plane. Allowable limits of damping ratios and undamped natural frequencies are therefore represented by allowable areas (that is, FQC regions) in the complex plane which are bounded by radial lines and circular arcs. For convenience, the real and imaginary axes of the complex plane will have the units σt^* and $i\omega t^*$, respectively.

Phugoid Flying Qualities

Because the phugoid is such a long-period mode, its flying qualities are specified in terms of damping-ratio limits only. For the particular level, category, and classification of the present study, the damping-ratio limits are (ref. 15)

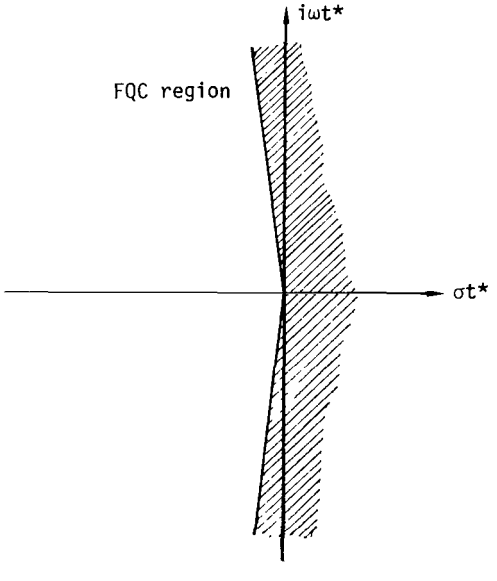

Sketch (b)

$$\zeta \geqq 0.04 \tag{A1}$$

which corresponds to phugoid roots located within the (unshaded) FQC region. The phugoid FQC region in sketch (b) is the same for any Mach number.

APPENDIX A

Short-Period Flying Qualities

Short-period flying qualities are specified in terms of both damping-ratio and undamped-natural-frequency limits. For the particular level, category, and classification of the present study, the damping-ratio limits are (ref. 15)

$$2.00 \geqq \zeta \geqq 0.30 \tag{A2}$$

The undamped-natural-frequency limits are functions of the quantity n_z/α, which is expressed in reference 17 as

$$\frac{n_z}{\alpha} = \frac{u_o}{g} \frac{Z_\delta M_w - M_\delta Z_w}{M_\delta - \frac{1}{u_o} Z_\delta M_q} \tag{A3}$$

After nondimensionalizing the aerodynamic coefficients and simplifying the resulting expression, equation (A3) becomes

$$\frac{n_z}{\alpha} = \frac{qS}{mg} C_{L_\alpha} \tag{A4}$$

For the particular level, category, and classification of the present study, reference 15 presents a figure similar to the following sketch (sketch (c)) for specifying the undamped-natural-frequency limits

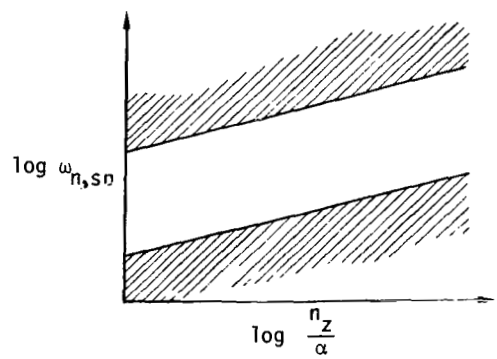

Sketch (c)

The curves defining the upper and lower frequency limits are straight lines, each with a slope of +1/2 on the log-log plot. Such a slope suggests the following equations for calculating the upper and lower limits of $\omega_{n,sp}$ in terms of n_z/α

$$\left(\omega_{n,sp}\right)_u = C_1\sqrt{\frac{n_z}{\alpha}} \tag{A5}$$

$$\left(\omega_{n,sp}\right)_\ell = C_2\sqrt{\frac{n_z}{\alpha}} \tag{A6}$$

where C_1 and C_2 are constants. When equation (A4) is substituted into equations (A5) and (A6), the upper and lower limits of $\omega_{n,sp}$ are expressed as

$$\left(\omega_{n,sp}\right)_u = C_1 u_o\sqrt{\frac{\rho S}{2mg} C_{L_\alpha}} \tag{A7}$$

$$\left(\omega_{n,sp}\right)_\ell = C_2 u_o\sqrt{\frac{\rho S}{2mg} C_{L_\alpha}} \tag{A8}$$

Equations (A7) and (A8) indicate that for an airplane of fixed geometry and fixed weight flying at constant altitude (which is the case in this study), a change in flight Mach number will result in changes in u_o and C_{L_α}. The changes in u_o and C_{L_α} result in different upper and lower limits of $\omega_{n,sp}$ at each Mach number.

Multiplying both sides of equations (A7) and (A8) by $t^*\left(=\frac{\bar{c}}{2u_o}\right)$ expresses the frequency limits in terms of undamped natural reduced frequencies

$$\left(k_{n,sp}\right)_u = \left(\omega_{n,sp}\right)_u t^* = C_1 \frac{\bar{c}}{2}\sqrt{\frac{\rho S}{2mg} C_{L_\alpha}} \tag{A9}$$

$$\left(k_{n,sp}\right)_\ell = \left(\omega_{n,sp}\right)_\ell t^* = C_2 \frac{\bar{c}}{2}\sqrt{\frac{\rho S}{2mg} C_{L_\alpha}} \tag{A10}$$

Equations (A9) and (A10) indicate that for an airplane of fixed geometry and fixed weight flying at constant altitude, a change in flight Mach number will result in changes in C_{L_α} only. The upper and lower limits of $k_{n,sp}$ at one Mach number may be expressed in terms of the upper and lower limits of $k_{n,sp}$ at another Mach number by

$$\left(k_{n,sp}\right)_{u_2} = \left(k_{n,sp}\right)_{u_1}\sqrt{\frac{C_{L_{\alpha,2}}}{C_{L_{\alpha,1}}}} \tag{A11}$$

$$\left(k_{n,sp}\right)_{\ell_2} = \left(k_{n,sp}\right)_{\ell_1}\sqrt{\frac{C_{L_{\alpha,2}}}{C_{L_{\alpha,1}}}} \tag{A12}$$

In the present study the square roots of the ratio of the lift-curve slopes in equations (A11) and (A12) are very close to unity (0.93), and consequently the upper and lower limits of $k_{n,sp}$ at the two Mach numbers of this study are very nearly equal. Therefore, for simplicity and consistent with other assumptions made in the study, the upper and lower limits of $k_{n,sp}$ at the two Mach numbers are assumed to be equal and resulted in the single short-period (unshaded) FQC region for both Mach numbers shown in sketch (d).

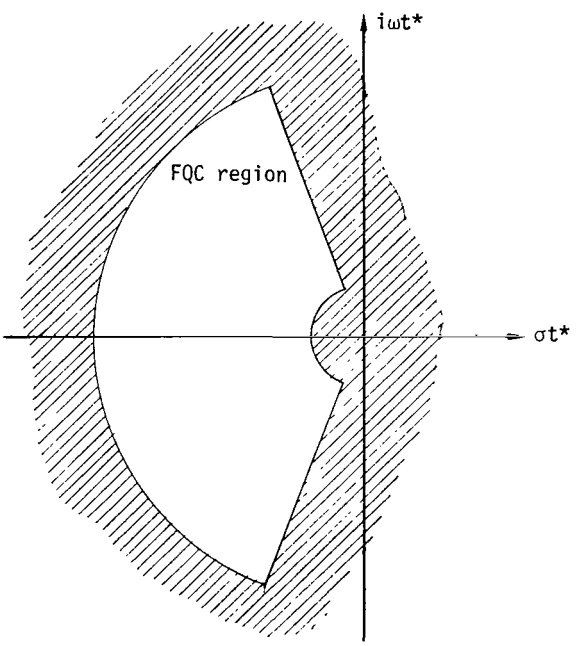

Sketch (d)

The short-period FQC region in sketch (d) is the same for any Mach number.

APPENDIX B

EFFECT OF FEEDBACK GAINS ON MANEUVERABILITY

The purpose of this appendix is to define maneuverability and to show the effect of feedback gains K_{α} and $K_{\dot{\theta}}$ on the apparent elevator angle per g (the maneuverability parameter of this study).

Maneuverability

The cases of actual and apparent maneuverability for conventional (statically stable) airplanes and for airplanes with relaxed static stability are considered in this section of the appendix. Maneuverability in the longitudinal degrees of freedom usually is defined by the elevator angle per g, which is the elevator deflection required to trim the airplane in steady accelerated flight (such as a steady pull-up maneuver) of constant load factor. This deflection $\Delta\delta/\Delta n$ is related to the control-stick deflection per g $(\Delta\delta_S/\Delta n)$ through the gear ratio K_{δ}

$$\frac{\Delta\delta}{\Delta n} = K_{\delta}\frac{\Delta\delta_S}{\Delta n} \tag{B1}$$

Sketch (e) illustrates the deflections of equation (B1) for a statically stable configuration and sketch (f) illustrates the deflections for a configuration with relaxed static stability without a static stability augmentation system (SSAS).

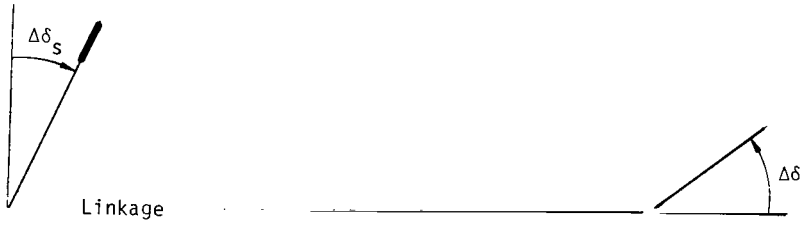

Sketch (e)

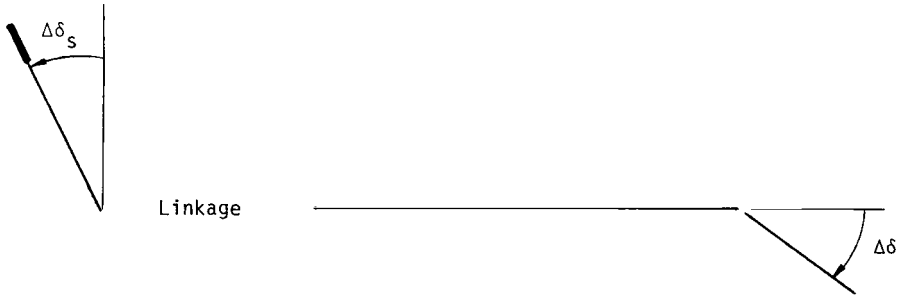

Sketch (f)

APPENDIX B

For a configuration with relaxed static stability and with an SSAS, a part of the required elevator deflection is provided by the SSAS, which permits the control stick to be deflected in the conventional sense. This condition is described by the following equation:

$$\frac{\Delta\delta}{\Delta n} = K_\delta \frac{\Delta\delta_s}{\Delta n} + K_\alpha \frac{\Delta\alpha}{\Delta n} + K_{\dot\theta} \frac{\Delta\dot\theta}{\Delta n} \tag{B2}$$

Equation (B2) is illustrated in sketch (g), where the pilot-commanded deflection $\Delta\delta_1 = K_\delta \Delta\delta_s$ and the SSAS-commanded deflection $\Delta\delta_2 = K_\alpha \Delta\alpha + K_{\dot\theta} \Delta\dot\theta$

Sketch (g)

For both the conventional configuration without an SSAS, illustrated in sketch (e), and the configuration with relaxed static stability with an SSAS, illustrated in sketch (g), the control-stick deflection is in the conventional sense for a steady pull-up maneuver. From equation (B1), the control-stick deflection per g is

$$\frac{\Delta\delta_s}{\Delta n} = \frac{1}{K_\delta} \frac{\Delta\delta}{\Delta n} \tag{B3}$$

and is a measure of the actual maneuverability. From equation (B2), the control-stick deflection per g is

$$\frac{\Delta\delta_s}{\Delta n} = \frac{1}{K_\delta}\left(\frac{\Delta\delta}{\Delta n} - K_\alpha \frac{\Delta\alpha}{\Delta n} - K_{\dot\theta} \frac{\Delta\dot\theta}{\Delta n}\right) \tag{B4}$$

where

$$\left(\frac{\Delta\delta}{\Delta n} - K_\alpha \frac{\Delta\alpha}{\Delta n} - K_{\dot\theta} \frac{\Delta\dot\theta}{\Delta n}\right) = \frac{\Delta\delta'}{\Delta n}$$

so that equation (B4) takes the form

$$\frac{\Delta\delta_s}{\Delta n} = \frac{1}{K_\delta}\frac{\Delta\delta'}{\Delta n} \tag{B5}$$

The quantity $\Delta\delta'/\Delta n$ is an apparent elevator deflection, which is taken to be a measure of apparent maneuverability. If feedback gains K_α and $K_{\dot\theta}$ are zero, equations (B4) and (B5) are measures of the actual maneuverability.

The actual elevator angle per g, $\Delta\delta/\Delta n$ in equation (B3), is expressed as

$$\frac{\Delta\delta}{\Delta n} = \frac{C_{L,o}}{C_{z_\delta}}\frac{h_m - h}{\frac{\ell_t}{\bar c} - (h_n - h)} \tag{B6}$$

Equation (B6) is obtained by algebraically manipulating a similar expression in reference 12. The quantities $C_{L,o}$ and C_{z_δ} are stability derivatives; $\ell_t/\bar c$ is the nondimensional tail length; and h_m, h_n, and h are the locations of the maneuver point, neutral point, and center of gravity in terms of fractions of the wing mean aerodynamic chord. The quantities $h_m - h$ and $h_n - h$ are the maneuver margin and static margin, also in terms of fractions of the wing mean aerodynamic chord.

The apparent elevator angle per g, $\Delta\delta'/\Delta n$ in equation (B5), may be expressed in terms of an apparent maneuver point and an apparent neutral point and expressed in a form similar to equation (B6)

$$\frac{\Delta\delta'}{\Delta n} = \frac{C_{L,o}}{C_{z_\delta}}\frac{h'_m - h}{\frac{\ell_t}{\bar c} - (h'_n - h)} \tag{B7}$$

The quantities h'_m and h'_n are the apparent maneuver point and the apparent neutral point and the quantities $h'_m - h$ and $h'_n - h$ are the apparent maneuver margin and the apparent static margin, all in terms of the wing mean aerodynamic chord. It remains to be shown that the apparent maneuver and neutral points are functions of the actual maneuver and neutral points and feedback gains K_α and $K_{\dot\theta}$.

Equations of Motion

The equations of motion (eq. (1)), including the control law (eq. (2) and the last row in eq. (1)), are simplified and manipulated in this section of the appendix. Expressions

for the apparent neutral point, the apparent maneuver point, and, ultimately, the apparent elevator angle per g are derived from these simplified and manipulated equations later in the appendix.

The equations are simplified by employing the short-period approximation (which eliminates the $\hat{u}$ variable) and by making the calm-atmosphere assumption (which eliminates α_g). An additional simplification is made in the control law, which is written here in terms of circular frequency and with the $\hat{u}$ and α_g terms removed

$$\delta = \frac{1}{1 + i\omega t_1}\left[K_\alpha(\alpha) + K_{\dot{\theta}}(i\omega\theta)\right] \tag{B8}$$

It is assumed that at the frequencies of interest (the short period having the highest), the quantity $i\omega t_1$ is sufficiently less than unity so that it may be set to zero. Written now in terms of the Laplace variable, the simplified control law is

$$\delta = K_\alpha(\alpha) + K_{\dot{\theta}}(s\theta) \tag{B9}$$

Equation (B9) now becomes the last row of the equations of motion. As a consequence of the short-period and calm-atmosphere assumptions, the equations of motion have been reduced from a system of four simultaneous equations (in variables $\hat{u}$, α, θ, and δ) with gust input on the right-hand side to a system of three simultaneous equations (in variables α, θ, and δ) with no gust input.

This system of three simultaneous equations (in variables α, θ, and δ) is manipulated into a system of two simultaneous equations (in variables α and θ) in the following manner: the simplified control law (eq. (B9)) is removed from the system of equations, which leaves two equations in three variables; equation (B9) is then substituted for δ in the remaining two equations and the following system of two simultaneous equations (in variables α and θ) results:

$$\left[\begin{array}{c|c} 2\mu t^* s - C_{Z_\alpha} & \left(-2\mu - C_{Z_q}\right)t^* s \\ -C_{Z_{\dot{\alpha}}} t^* s \boxed{\frac{1 - e^{-\tau s}}{\tau s}} - C_{Z_\delta} K_\alpha & -C_{Z_\delta} K_{\dot{\theta}} s \\ \hline -C_{m_\alpha} & i_B t^{*2} s^2 - C_{m_q} t^* s \\ -C_{m_{\dot{\alpha}}} t^* s \boxed{\frac{1 - e^{-\tau s}}{\tau s}} - C_{m_\delta} K_\alpha & -C_{m_\delta} K_{\dot{\theta}} s \end{array}\right] \left\{\begin{array}{c} \alpha \\ \theta \end{array}\right\} = \left\{\begin{array}{c} 0 \\ 0 \end{array}\right\} \tag{B10}$$

APPENDIX B

Apparent stability derivatives within equation (B10) are defined in terms of the stability derivatives and feedback gains as

$$C'_{z_\alpha} = C_{z_\alpha} + C_{z_\delta} K_\alpha \tag{B11}$$

$$C'_{z_q} = C_{z_q} + C_{z_\delta} K_{\dot\theta} \frac{1}{t^*} \tag{B12}$$

$$C'_{m_\alpha} = C_{m_\alpha} + C_{m_\delta} K_\alpha \tag{B13}$$

$$C'_{m_q} = C_{m_q} + C_{m_\delta} K_{\dot\theta} \frac{1}{t^*} \tag{B14}$$

When equations (B11) to (B14) are substituted into equation (B10), it becomes

$$\begin{bmatrix} 2\mu t^* s - C'_{z_\alpha} & \left(-2\mu - C'_{z_q}\right) t^* s \\ -C_{z_{\dot\alpha}} t^* s \left[\frac{1 - e^{-\tau s}}{\tau s}\right] & \\ -C'_{m_\alpha} & i_B t^{*2} s^2 - C'_{m_q} t^* s \\ -C_{m_{\dot\alpha}} t^* s \left[\frac{1 - e^{-\tau s}}{\tau s}\right] & \end{bmatrix} \begin{Bmatrix} \alpha \\ \theta \end{Bmatrix} = \begin{Bmatrix} 0 \\ 0 \end{Bmatrix} \tag{B15}$$

The equations of motion expressed by equation (B15) are now in proper form for deriving expressions for the apparent neutral point, the apparent maneuver point, and the apparent elevator angle per g in terms of feedback gains K_α and $K_{\dot\theta}$.

Apparent Neutral Point

The derivation of the expression for h'_n as a function of K_α and a discussion of the effect of K_α on h'_n are presented in this section. The actual neutral point appears within the following expression (ref. 12) for C_{m_α}, the static stability derivative,

$$C_{m_\alpha} = C_{L_\alpha}\left(h - h_n\right) \tag{B16}$$

Similarly, the apparent neutral point appears within the expression for C'_{m_α}, the apparent static stability derivative,

$$C'_{m_\alpha} = C_{L_\alpha}\left(h - h'_n\right) \tag{B17}$$

Substituting equation (B16) into equation (B13), equating equations (B13) and (B17), and then solving for h'_n gives the following expression for the apparent neutral point in terms of the actual neutral point and feedback gain K_α:

$$h'_n = h_n - \frac{C_{m_\delta}}{C_{L_\alpha}} K_\alpha \tag{B18}$$

From equation (B18) it is clear that when K_α is zero, the apparent and actual neutral points are the same. However, as K_α increases, the apparent neutral point moves aft; this movement is stabilizing for a configuration which is initially statically unstable.

Figure 12 contains plots of the apparent neutral point and the apparent static margin as functions of K_α for both statically unstable configurations and both flight conditions. The originally statically unstable configurations become statically stable at values of K_α for which the apparent static margin becomes positive. Because the C_{m_δ} stability derivative is directly proportional to the area of the horizontal tail (all other parameters constant), the slope of h'_n as a function of K_α is also directly proportional to the area of the horizontal tail (all other parameters constant). This dependence on tail area accounts for the shallower slopes on the plots of h'_n against K_α for the reduced-unstable configuration. It also accounts for the larger values of K_α required for stability for the reduced-unstable configuration.

Apparent Maneuver Point

The derivation of the expression for h'_m as a function of K_α and $K_{\dot\theta}$ and a discussion of the effects of K_α and $K_{\dot\theta}$ on h'_m are presented this section.

From the expansion of the stability determinant of equation (B15) the following expression is satisfied only when the short-period mode is neutrally stable (that is, when the center of gravity is at the maneuver point) (ref. 12)

$$C'_{z_\alpha} C'_{m_q} = 2\mu C'_{m_\alpha} \tag{B19}$$

When equations (B11), (B13), and (B14) are substituted into equation (B19), the following expression results:

$$\left(C_{z_\alpha} + C_{z_\delta}K_\alpha\right)\left(C_{m_q} + C_{m_\delta}K_{\dot\theta}\frac{1}{t^*}\right) = 2\mu\left(C_{m_\alpha} + C_{m_\delta}K_\alpha\right) \tag{B20}$$

When equation (B16) and the following approximation (ref. 12) are substituted into equation (B20),

$$C_{z_\alpha} \doteq -C_{L_\alpha}$$

the following equation results:

$$-C_{L_\alpha}C_{m_q} + \left(-C_{L_\alpha}C_{m_\delta}K_{\dot\theta}\frac{1}{t^*} + C_{m_q}C_{z_\delta}K_\alpha + C_{z_\delta}C_{m_\delta}K_\alpha K_{\dot\theta}\frac{1}{t^*}\right)$$
$$= 2\mu C_{L_\alpha}\left(h - h_n\right) + 2\mu C_{m_\delta}K_\alpha \tag{B21}$$

Equation (B21) is satisfied only when the center of gravity is located at the maneuver point h_m or, in this case, the apparent maneuver point h'_m. Substituting h'_m for h in equation (B21) and solving for h'_m gives the following expression for the apparent maneuver point:

$$h'_m = \left(h_n - \frac{C_{m_q}}{2\mu}\right) + \frac{1}{2\mu C_{L_\alpha}}\left(C_{m_q}C_{z_\delta}K_\alpha - 2\mu C_{m_\delta}K_\alpha + C_{z_\delta}C_{m_\delta}K_\alpha K_{\dot\theta}\frac{1}{t^*} - C_{L_\alpha}C_{m_\delta}K_{\dot\theta}\frac{1}{t^*}\right) \tag{B22}$$

The actual maneuver point is expressed as a function of the actual neutral point as (ref. 12)

$$h_m = h_n - \frac{C_{m_q}}{2\mu} \tag{B23}$$

When equation (B23) is substituted into equation (B22), the apparent maneuver point is expressed as a function of the actual maneuver point and feedback gains K_α and $K_{\dot\theta}$

$$h'_m = h_m + \frac{1}{2\mu C_{L_\alpha}}\left(C_{m_q}C_{z_\delta}K_\alpha - 2\mu C_{m_\delta}K_\alpha + C_{z_\delta}C_{m_\delta}K_\alpha K_{\dot\theta}\frac{1}{t^*} - C_{L_\alpha}C_{m_\delta}K_{\dot\theta}\frac{1}{t^*}\right) \tag{B24}$$

Equation (B24) indicates that when K_α and $K_{\dot\theta}$ are both zero, the apparent and actual maneuver points are the same. However, as K_α or $K_{\dot\theta}$ or both increase, the apparent maneuver point moves aft.

Figure 13 contains plots of the apparent maneuver point and the apparent maneuver margin as functions of K_α and $K_{\dot\theta}$ for both statically unstable configurations and both flight conditions. The solid curves represent variations in K_α with $K_{\dot\theta}$ equal to zero and the dashed curves represent variations in $K_{\dot\theta}$ with K_α equal to zero. A surface would be necessary to show the effects of varying K_α and $K_{\dot\theta}$ simultaneously. Figure 13 shows that the apparent maneuver point is more sensitive to $K_{\dot\theta}$ than to K_α and that the slopes of the curves are shallower for the reduced-unstable configurations and reflect the dependence of h'_m on tail area.

Apparent Elevator Angle per g

A discussion of the effects of K_α and $K_{\dot\theta}$ on $\Delta\delta'/\Delta n$ is presented in this section.

The expression for the apparent elevator angle per g in terms of the apparent maneuver point and the apparent neutral point was presented in equation (B7) and repeated here

$$\frac{\Delta\delta'}{\Delta n} = \frac{C_{L,o}}{C_{z_\delta}} \frac{h'_m - h}{\frac{\ell_t}{\bar{c}} - \left(h'_n - h\right)} \tag{B25}$$

Equations (B18) and (B24) of the previous two sections show that the apparent neutral point h'_n is a function of feedback gain K_α and that the apparent maneuver point h'_m is a function of feedback gains K_α and $K_{\dot\theta}$. Thus, the apparent elevator angle per g is a function of feedback gains K_α and $K_{\dot\theta}$. Because h'_m and h'_n reduce to h_m and h_n when both feedback gains are zero, the apparent elevator angle per g reduces to the actual elevator angle per g when both feedback gains are zero.

Figure 14 contains plots of the apparent elevator angle per g as functions of K_α and $K_{\dot\theta}$ for both statically unstable configurations and both flight conditions. The solid curves represent variations in K_α with $K_{\dot\theta}$ equal to zero and the dashed curves represent variations in $K_{\dot\theta}$ with K_α equal to zero. A surface would be necessary to show the effects of varying K_α and $K_{\dot\theta}$ simultaneously. Figure 14 shows that the apparent elevator angle per g is more sensitive to $K_{\dot\theta}$ than to K_α and that, contrary to figures 12 and 13, the slopes of the curves show very little dependence on tail area, but show considerable dependence on Mach number. A comparison of figures 13 and 14 shows that, as predicted, the apparent elevator angle per g becomes negative at the same values of gain at which the apparent maneuver margin becomes positive.

REFERENCES

1. Perry, Boyd, III: The Effects of an Autopilot on Airplane Responses to Turbulence With Emphasis on Tail Loads. NASA TN D-7231, 1973.

2. Porter, Richard F.; Loomis, James P.; and Robinson, Alfred C.: A Procedure for Assessing Aircraft Turbulence-Penetration Performance. NASA CR-1510, 1970.

3. Oehman, Waldo I.: An Analytical Study of Airplane-Autopilot Response to Atmospheric Turbulence. NASA TN D-6869, 1972.

4. Dempster, John B.; and Roger, Kenneth L.: Evaluation of B-52 Structural Response to Random Turbulence With Stability Augmentation Systems. J. Aircraft, vol. 4, no. 6, Nov.-Dec. 1967, pp. 507-512.

5. Bulban, Erwin J.: YF-16 Stresses Advanced Technology. Aviation Week & Space Technol., vol. 100, no. 1, Jan. 7, 1974, pp. 40-48.

6. Fink, Donald E.: YF-17 Evolved From Previous Data Base. Aviation Week & Space Technol., vol. 100, no. 15, Apr. 15, 1974, pp. 46-51.

7. Tomlinson, Lloyd R.: Control System Design Considerations for a Longitudinally Unstable Supersonic Transport. J. Aircraft, vol. 10, no. 10, Oct. 1973, pp. 594-601.

8. Strahota, R. A.; and McGovern, D. R.: Combat Control Verstility With CCV. AIAA Paper No. 73-160, Jan. 1973.

9. Anderson, D. C.; Berger, R. L. ; and Hess, J. R., Jr.: Maneuver Load Control and Relaxed Static Stability Applied to a Contemporary Fighter Aircraft. AIAA Paper No. 72-870, Aug. 1972.

10. Martin, Clark: Advanced Fighter Technology Entry Set. Aviation Week & Space Technol., vol. 99, no. 8, Aug. 20, 1973, pp. 14-16.

11. Kass, Gerald J.; and Johannes, Robert P.: B-52 Control Configured Vehicles Program. AIAA Paper No. 72-747, Aug. 1972.

12. Etkin, Bernard: Dynamics of Flight. John Wiley & Sons, Inc., c.1959.

13. Blakelock, John H.: Automatic Control of Aircraft and Missiles. John Wiley & Sons, Inc., c.1965.

14. Houbolt, John C.; Steiner, Roy; and Pratt, Kermit G.: Dynamic Response of Airplanes to Atmospheric Turbulence Including Flight Data on Input and Response. NASA TR R-199, 1964.

15. Flying Qualities of Piloted Airplanes. Mil. Specif. MIL-F-8785B (ASG), August 7, 1969.

16. Pasley, Lewis H.; Rohling, Walter J.; and Wattman, Walter J.: Compatibility of Maneuver Load Control and Relaxed Static Stability. AIAA Paper No. 73-791, Aug. 1973.

17. Chalk, C. R.; and Wilson, R. K.: Airplane Flying Qualities Specification Revision. J. Aircraft, vol. 6, no. 3, May-June 1969, pp. 232-239.

TABLE I.- PHYSICAL DIMENSIONS OF EXAMPLE CONFIGURATIONS

Quantity	Configuration		
	Baseline	Nominal unstable	Reduced unstable
Mass of airplane, m, kg	5 730	5 730	5 444
Pitch moment of inertia, I_{YY}, kg-m^2	35 766	34 953	35 419
Wing span, b, m	13.54	13.54	13.54
Wing mean aerodynamic chord, $\bar{c}$, m	2.55	2.55	2.55
Wing area, S, m^2	31.8	31.8	31.8
Sweep angle of wing quarter chord, $\Lambda_{.25}$, deg	28.6	28.6	28.6
Horizontal-tail span, b_t, m	5.35	5.35	3.78
Horizontal-tail mean aerodynamic chord, $\bar{c}_t$, m	1.47	1.47	1.04
Horizontal-tail area, S_t, m^2	7.16	7.16	3.58
Sweep angle of horizontal-tail 40 percent chord, Λ_t, deg	26.5	26.5	26.5
Tail length, ℓ_t, m	5.10	4.85	4.54
Elevator chord ratio	0.35	0.35	0.35
Elevator servo characteristic time, t_1, sec	0.066	0.066	0.066

TABLE II.- CENTER-OF-GRAVITY POSITION AND STABILITY PARAMETERS (IN FRACTION $\bar{c}$)

[Altitude = 6100 m]

Quantity	Mach number, 0.50			Mach number, 0.75		
	Baseline	Nominal unstable	Reduced unstable	Baseline	Nominal unstable	Reduced unstable
h	0.32	0.42	0.31	0.32	0.42	0.31
h_n	.38	.38	.27	.37	.37	.28
h_n - h	.06	-.04	-.04	.05	-.05	-.03
h_m	.40	.39	.28	.39	.39	.29
h_m - h	.08	-.03	-.03	.07	-.03	-.02

TABLE III.- STABILITY DERIVATIVES OF EXAMPLE CONFIGURATIONS

[Altitude = 6100 m]

Stability derivative	Mach number, 0.50			Mach number, 0.75		
	Baseline	Nominal unstable	Reduced unstable	Baseline	Nominal unstable	Reduced unstable
C_{x_u}	-0.040	-0.040	-0.040	-0.061	-0.061	-0.061
C_{x_α}	.102	.102	.100	.038	.038	.037
$C_{L,o}$	.216	.216	.205	.096	.096	.091
C_{z_u}	-.072	-.072	-.068	-.124	-.124	-.117
C_{z_α}	-4.80	-4.80	-4.66	-5.54	-5.54	-5.39
$C_{z_{\dot{\alpha}}}$	-1.65	-1.57	-.733	-2.22	-2.11	-.989
C_{z_q}	-3.46	-3.29	-1.54	-4.02	-3.81	-1.78
C_{z_δ}	-.502	-.502	-.251	-.583	-.583	-.291
C_{m_u}	0	0	0	0	0	0
C_{m_α}	-.287	.191	.186	-.276	.276	.161
$C_{m_{\dot{\alpha}}}$	-3.29	-2.97	-1.30	-4.44	-4.01	-1.76
C_{m_q}	-6.91	-6.23	-2.73	-8.02	-7.24	-3.17
C_{m_δ}	-1.00	-.953	-.446	-1.16	-1.11	-.517

TABLE IV.- STABILITY AND MANEUVERABILITY PARAMETERS FOR CONTROL LAW 1

[Altitude = 6100 m]

Mach number	Configuration	Feedback gains		Short period		Phugoid		$\Delta\delta^r/\Delta n$, deg/g
		K_α, rad/rad	$K_{\dot\theta}$, rad/rad/sec	k_o	ζ	k_o	ζ	
0.50	Baseline	0	0	1.73×10^{-2}	0.560	6.80×10^{-4}	0.058	-0.968
.50	Nominal unstable	.44	.03	1.70	.557	6.26	.062	-.952
.50	Reduced unstable	.88	.15	1.73	.557	5.99	.070	-1.896
.75	Baseline	0	0	1.61	.653	3.39	.198	-.333
.75	Nominal unstable	.41	.03	1.61	.640	2.77	.242	-.327
.75	Reduced unstable	.61	.11	1.63	.652	2.63	.267	-.634

TABLE V.- TURBULENCE RESPONSES FOR CONTROL LAW 1

[Altitude = 6100 m]

Mach number	Configuration	Feedback gains		Turbulence responses										
		K_α, $\frac{\text{rad}}{\text{rad}}$	$K_{\dot\theta}$, $\frac{\text{rad}}{\text{rad/sec}}$	$\bar{A}_{\hat u}$, $\frac{1}{\text{m/sec}}$	$\bar{A}_\alpha$, $\frac{\text{rad}}{\text{m/sec}}$	$\bar{A}_{\alpha_t}$, $\frac{\text{rad}}{\text{m/sec}}$	$\bar{A}_\theta$, $\frac{\text{rad}}{\text{m/sec}}$	$\bar{A}_{\dot\theta}$, $\frac{\text{rad/sec}}{\text{m/sec}}$	$\bar{A}_\delta$, $\frac{\text{rad}}{\text{m/sec}}$	$\bar{A}_{\Delta n}$, $\frac{\text{g units}}{\text{m/sec}}$	$\bar{A}_T$, $\frac{\text{N-m}}{\text{m/sec}}$	$\bar{A}_{M,b}$, $\frac{\text{N-m}}{\text{m/sec}}$	$\bar{A}_{C_T}$, $\frac{1}{\text{m/sec}}$	$\bar{A}_{C_{M,b}}$, $\frac{1}{\text{m/sec}}$
0.50	Baseline	0	0	3.77×10^{-3}	6.04×10^{-3}	1.45×10^{-3}	6.20×10^{-3}	3.45×10^{-3}	0	6.76×10^{-2}	19.6	81.4	2.28×10^{-4}	9.45×10^{-4}
.50	Nominal unstable	.44	.03	2.97	6.00	1.60	4.69	3.28	1.32×10^{-3}	7.45	22.2	143.7	2.58	1.67×10^{-3}
.50	Reduced unstable	.88	.15	3.23	6.04	1.50	4.99	3.12	2.46	7.28	7.34	67.6	2.41	2.23
.75	Baseline	0	0	6.56×10^{-4}	3.97	7.71×10^{-4}	2.10	2.59	0	1.12×10^{-1}	27.7	109.9	1.43	5.68×10^{-4}
.75	Nominal unstable	.41	.03	3.23	3.90	9.19	1.16	2.77	8.17×10^{-4}	1.29	33.8	217.1	1.75	1.12×10^{-3}
.75	Reduced unstable	.61	.11	4.49	3.90	8.23	1.45	2.13	1.09×10^{-3}	1.22	10.5	85.4	1.53	1.25

TABLE VI.- STABILITY AND MANEUVERABILITY PARAMETERS FOR CONTROL LAW 2

[Altitude = 6100 m]

Mach number	Configuration	Feedback gains		Short period		Phugoid		$\Delta\delta'/\Delta n$, deg/g
		K_α, rad/rad	$K_{\dot\theta}$, rad/rad/sec	k_o	ζ	k_o	ζ	
0.50	Baseline	0	0	1.73×10^{-2}	0.560	6.80×10^{-4}	0.058	-0.968
.50	Nominal unstable	.25	.11	----------	1.029	3.18	.161	-.725
.50	Reduced unstable	.60	.03	9.98×10^{-3}	.619	5.99	.057	-.718
.75	Baseline	0	0	1.61×10^{-2}	.653	3.39	.198	-.333
.75	Nominal unstable	.27	.06	----------	1.024	8.91×10^{-5}	.630	-.253
.75	Reduced unstable	.45	.02	9.47×10^{-3}	.682	2.80×10^{-4}	.244	-.253

TABLE VII.- TURBULENCE RESPONSES FOR CONTROL LAW 2

[Altitude = 6100 m]

Mach number	Configuration	Feedback gains		Turbulence responses										
		K_α, rad/rad	$K_{\dot\theta}$, rad/rad/sec	$\bar{A}_{\hat u}$, 1/m/sec	$\bar{A}_\alpha$, rad/m/sec	$\bar{A}_{\alpha_t}$, rad/m/sec	$\bar{A}_\theta$, rad/m/sec	$\bar{A}_{\dot\theta}$, rad/sec/m/sec	$\bar{A}_\delta$, rad/m/sec	$\bar{A}_{\Delta n}$, g units/m/sec	$\bar{A}_T$, N-m/m/sec	$\bar{A}_{M,b}$, N-m/m/sec	$\bar{A}_{C_T}$, 1/m/sec	$\bar{A}_{C_{M,b}}$, 1/m/sec
0.50	Baseline	0	0	3.77×10^{-3}	6.04×10^{-3}	1.45×10^{-3}	6.20×10^{-3}	3.45×10^{-3}	0	6.76×10^{-2}	19.6	81.4	2.28×10^{-4}	9.45×10^{-4}
.50	Nominal unstable	.25	.11	4.99×10^{-4}	5.51	1.73	8.14×10^{-4}	1.68	9.19×10^{-4}	7.74	23.6	136.1	2.75	1.59×10^{-3}
.50	Reduced unstable	.60	.03	2.59×10^{-3}	5.91	1.64	3.84×10^{-3}	1.94	1.85×10^{-3}	7.68	7.87	61.8	2.58	2.03
.75	Baseline	0	0	6.56×10^{-4}	3.97	7.71×10^{-4}	2.10	2.59	0	1.12×10^{-1}	27.7	109.9	1.43	5.68×10^{-4}
.75	Nominal unstable	.27	.06	3.51	3.67	9.91	1.10	2.30	6.59×10^{-4}	1.34	36.0	213.1	1.86	1.10×10^{-3}
.75	Reduced unstable	.45	.02	2.89	3.87	8.89	1.02	1.63	8.63	1.27	11.2	80.5	1.64	1.18

TABLE VIII.- STABILITY AND MANEUVERABILITY PARAMETERS FOR CONTROL LAW 3

[Altitude = 6100 m]

Mach number	Configuration	Feedback gains		Short period		Phugoid		$\Delta\delta'/\Delta n$, deg/g
		K_u, rad/m/sec	$K_{\dot\theta}$, rad/rad/sec	k_o	ζ	k_o	ζ	
0.50	Baseline	0	0	1.73×10^{-2}	0.560	6.80×10^{-4}	0.058	-0.968
.50	Nominal unstable	-1.3×10^{-4}	.30	4.79	.823	7.82×10^{-5}	.703	-.718
.50	Reduced unstable	-2.7	.46	2.26	.948	6.28	.833	-.738
.75	Baseline	0	0	1.61	.653	3.39×10^{-4}	.198	-.333
.75	Nominal unstable	-6.2×10^{-5}	.18	4.94	.719	5.94	.797	-.254
.75	Reduced unstable	-7.5	.20	2.38	.896	4.99	.858	-.244

TABLE IX.- TURBULENCE RESPONSES FOR CONTROL LAW 3

[Altitude = 6100 m]

Mach number	Configuration	Feedback gains		Turbulence responses										
		K_u, rad/m/sec	$K_{\dot\theta}$, rad/rad/sec	$\bar{A}_{\hat u}$, 1/m/sec	$\bar{A}_{\alpha}$, rad/m/sec	$\bar{A}_{\alpha_t}$, rad/m/sec	$\bar{A}_{\theta}$, rad/m/sec	$\bar{A}_{\dot\theta}$, rad/sec/m/sec	$\bar{A}_{\delta}$, rad/m/sec	$\bar{A}_{\Delta n}$, g units/m/sec	$\bar{A}_{T}$, N-m/m/sec	$\bar{A}_{M,b}$, N-m/m/sec	$\bar{A}_{C_T}$, 1/m/sec	$\bar{A}_{C_{M,b}}$, 1/m/sec
0.50	Baseline	0	0	3.77×10^{-3}	6.04×10^{-3}	1.45×10^{-3}	6.20×10^{-3}	3.45×10^{-3}	0	6.76×10^{-2}	19.6	81.4	2.28×10^{-4}	9.45×10^{-4}
.50	Nominal unstable	-1.3×10^{-4}	.30	4.10	4.99	1.97	4.76	2.63	7.41×10^{-4}	8.53	26.7	143.7	3.10	1.67×10^{-3}
.50	Reduced unstable	-2.7	.46	6.17	4.69	2.00	7.35	3.06	1.36×10^{-3}	8.89	9.43	61.8	3.10	2.03
.75	Baseline	0	0	6.56×10^{-4}	3.97	7.71×10^{-4}	2.10	2.59	0	1.12×10^{-1}	27.7	109.9	1.43	5.68×10^{-4}
.75	Nominal unstable	-6.2×10^{-5}	.18	1.56×10^{-3}	3.35	1.14×10^{-3}	4.17	3.44	5.77×10^{-4}	1.48	40.8	226.0	2.11	1.17×10^{-3}
.75	Reduced unstable	-7.5	.20	1.84	3.25	1.07	4.82	3.16	6.10	1.43	13.2	80.1	1.93	1.17

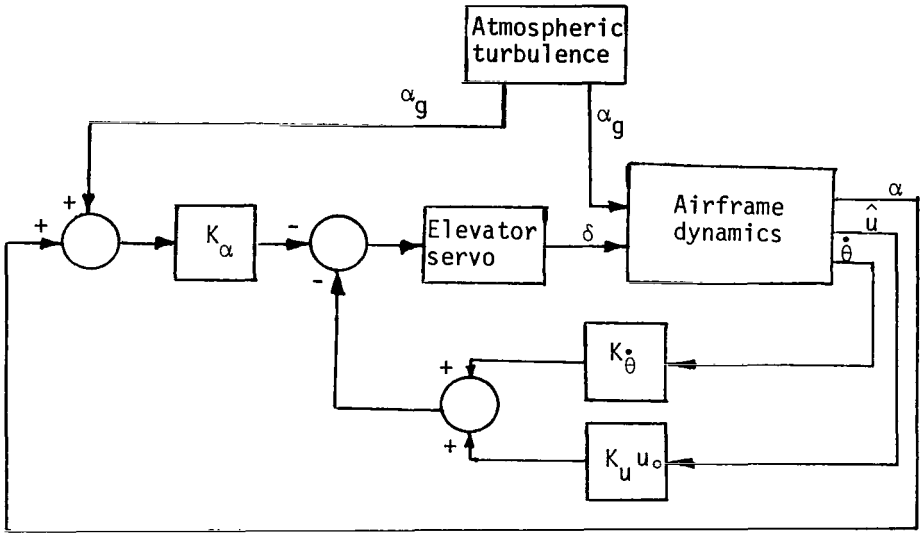

Figure 1.- Block diagram of airplane-SSAS system.

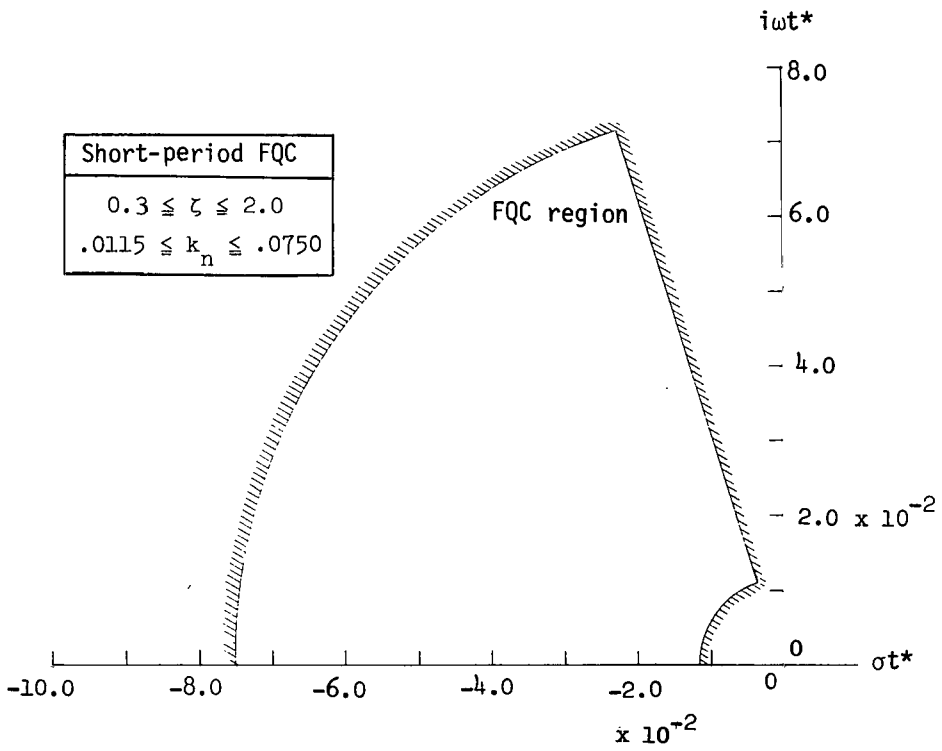

(a) Short-period region.

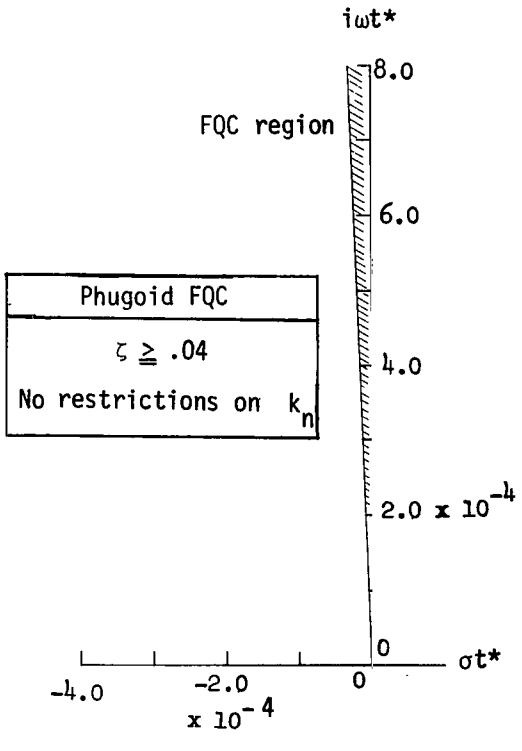

(b) Phugoid region.

Figure 2.- Flying qualities criteria regions.

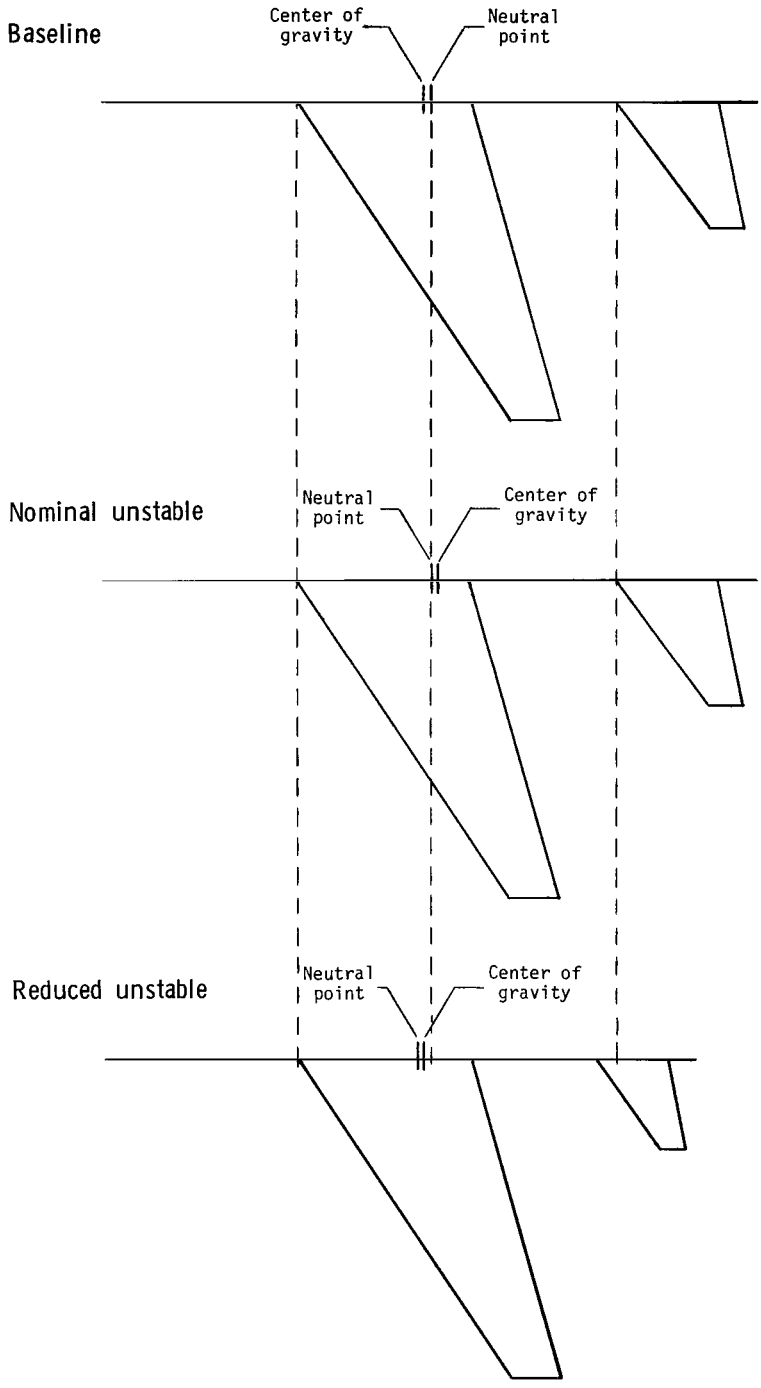

Figure 3.- Comparison of vehicle configurations.

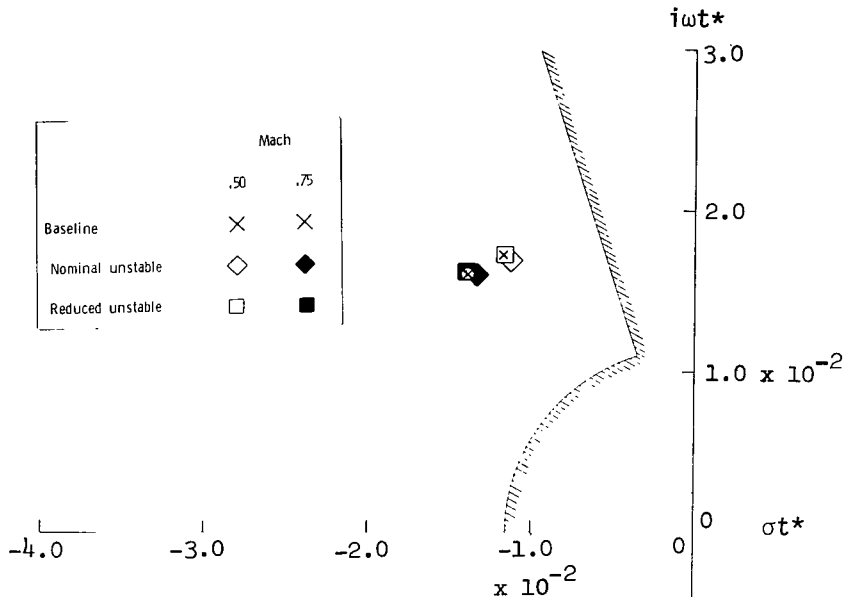

(a) Short-period roots.

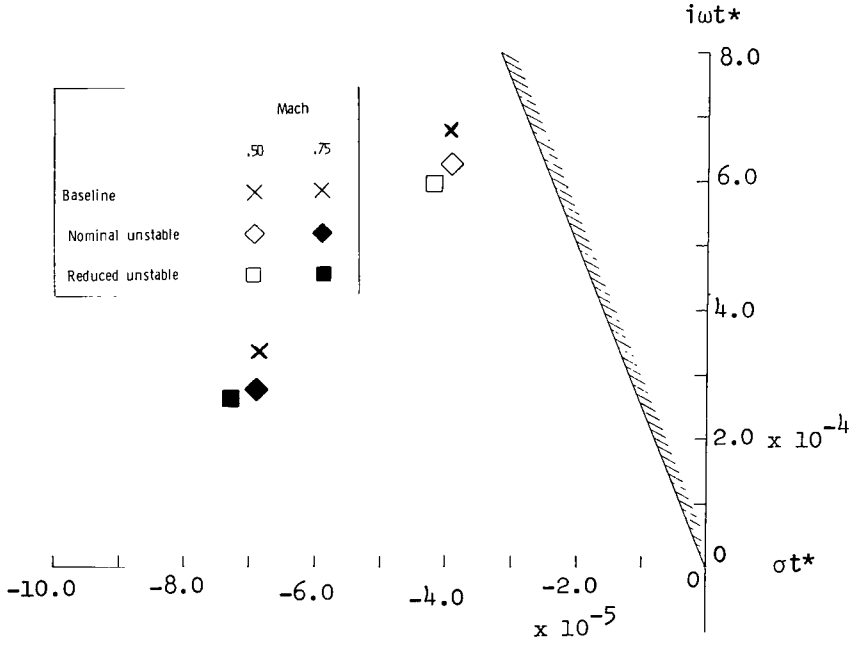

(b) Phugoid roots.

Figure 4.- Roots of longitudinal modes for control law 1.

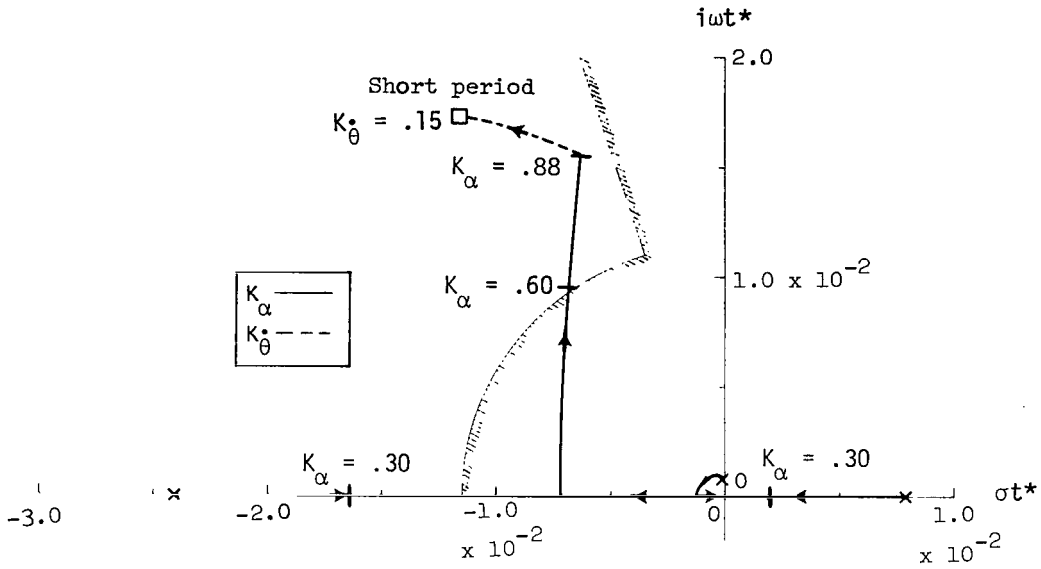

(a) Short-period locus.

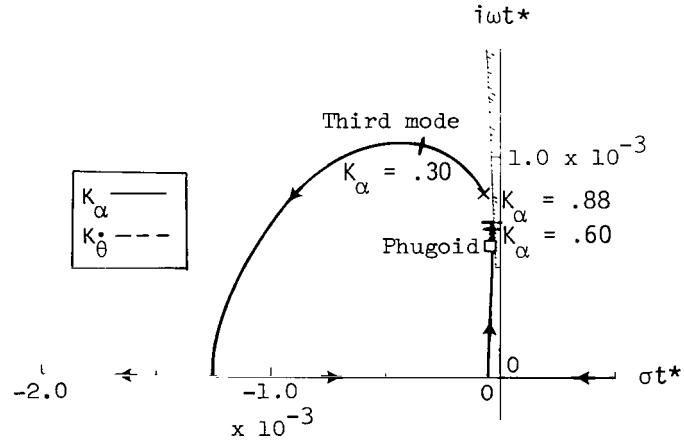

(b) Phugoid locus.

Figure 5.- Typical root locus for control law 1. Reduced-unstable configuration; M = 0.50.

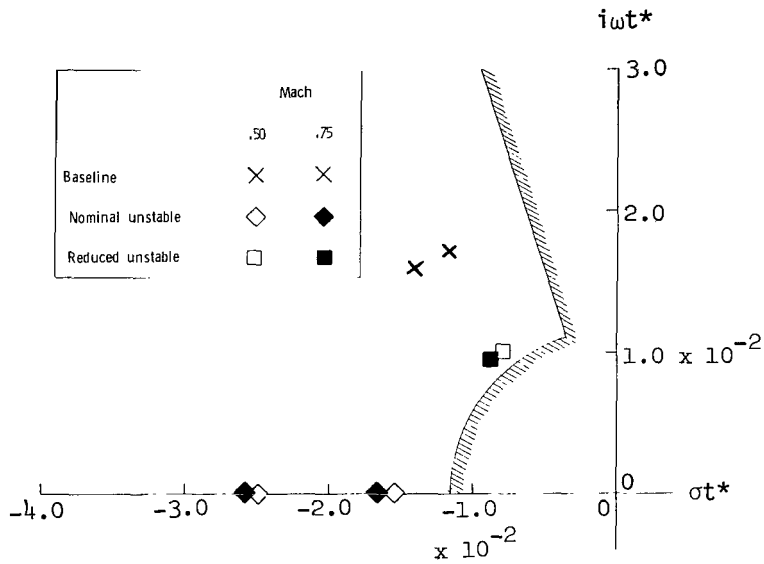

(a) Short-period roots.

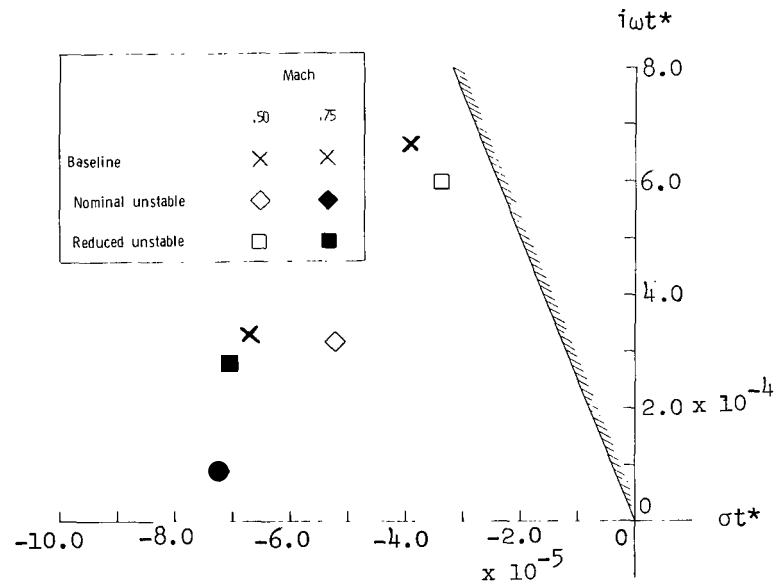

(b) Phugoid roots.

Figure 6.- Roots of longitudinal modes for control law 2.

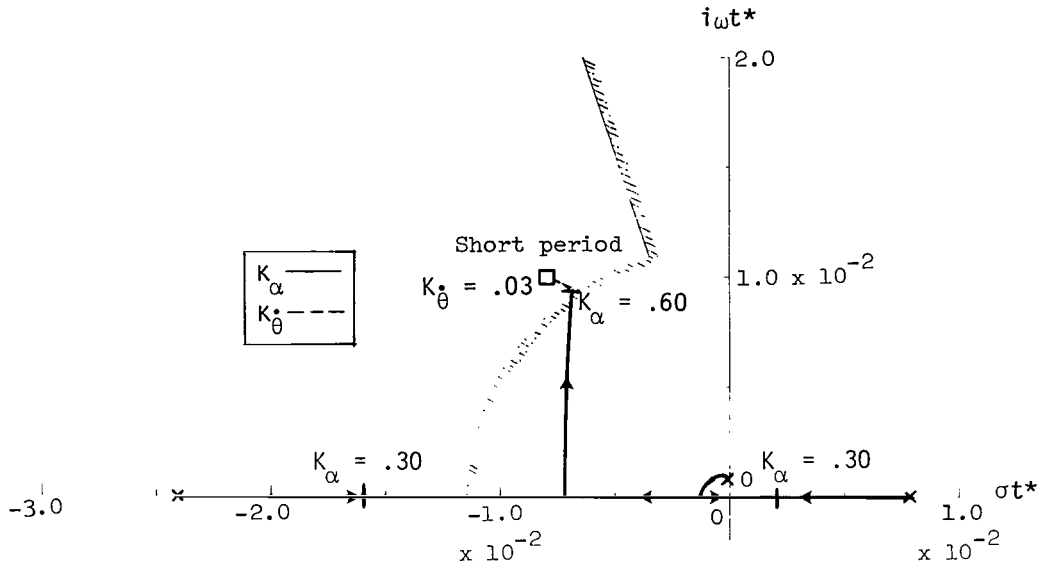

(a) Short-period locus.

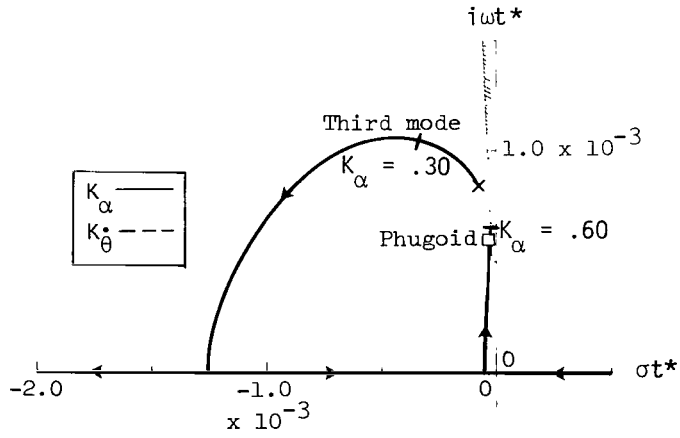

(b) Phugoid locus.

Figure 7.- Typical root locus for control law 2. Reduced-unstable configuration; M = 0.50.

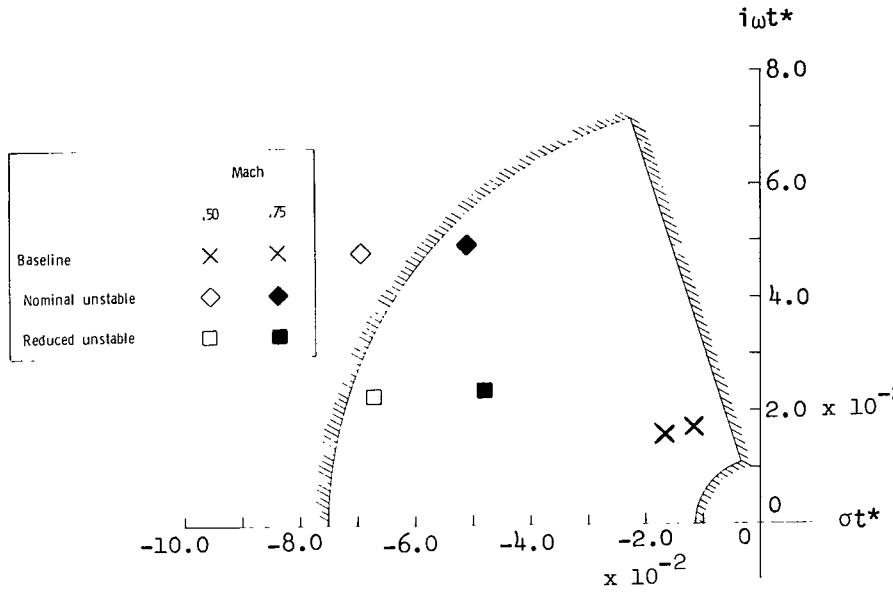

(a) Short-period roots.

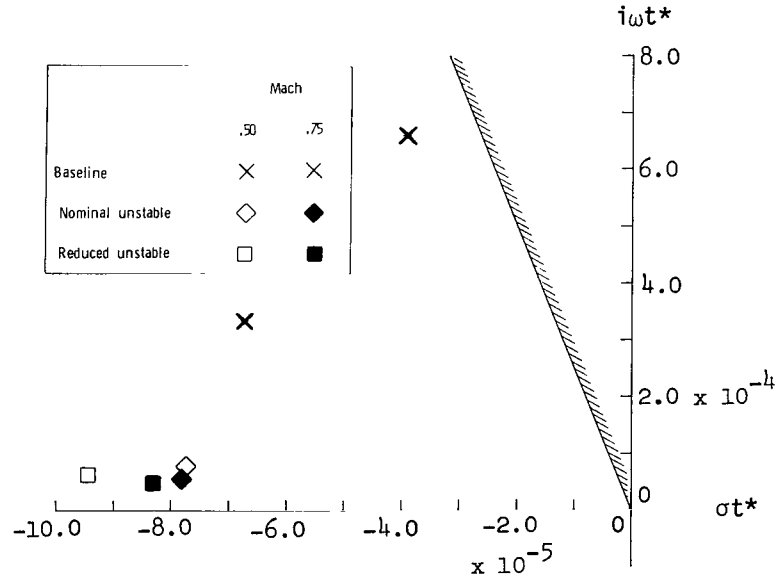

(b) Phugoid roots.

Figure 8.- Roots of longitudinal modes for control law 3.

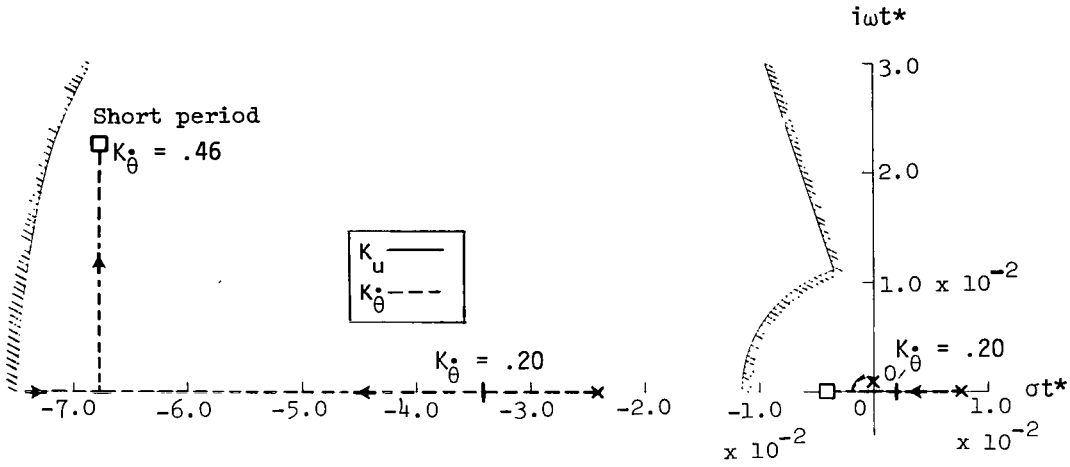

(a) Short-period locus.

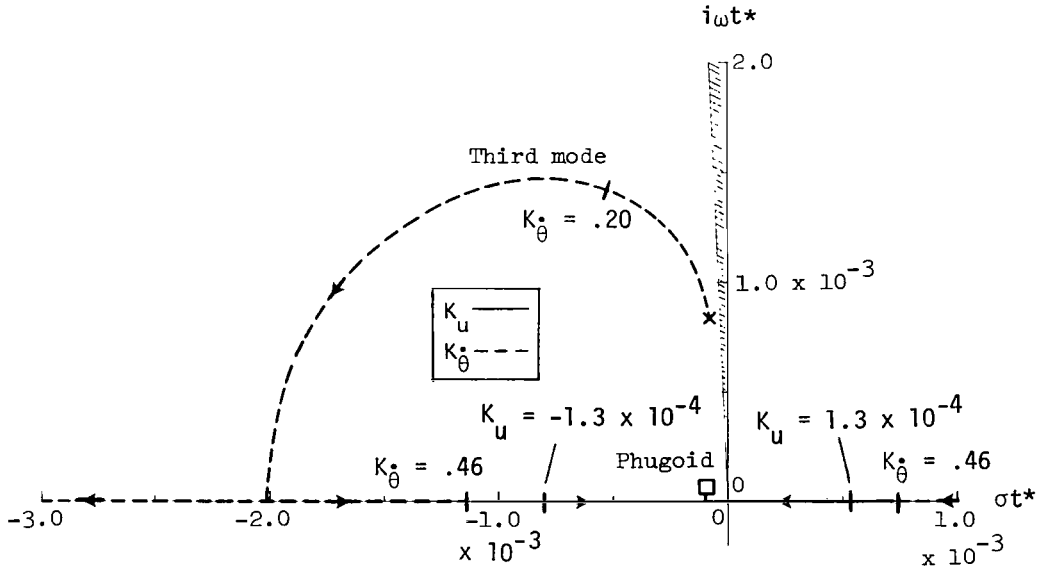

(b) Phugoid locus.

Figure 9.- Typical root locus for control law 3. Reduced-unstable configuration; M = 0.50.

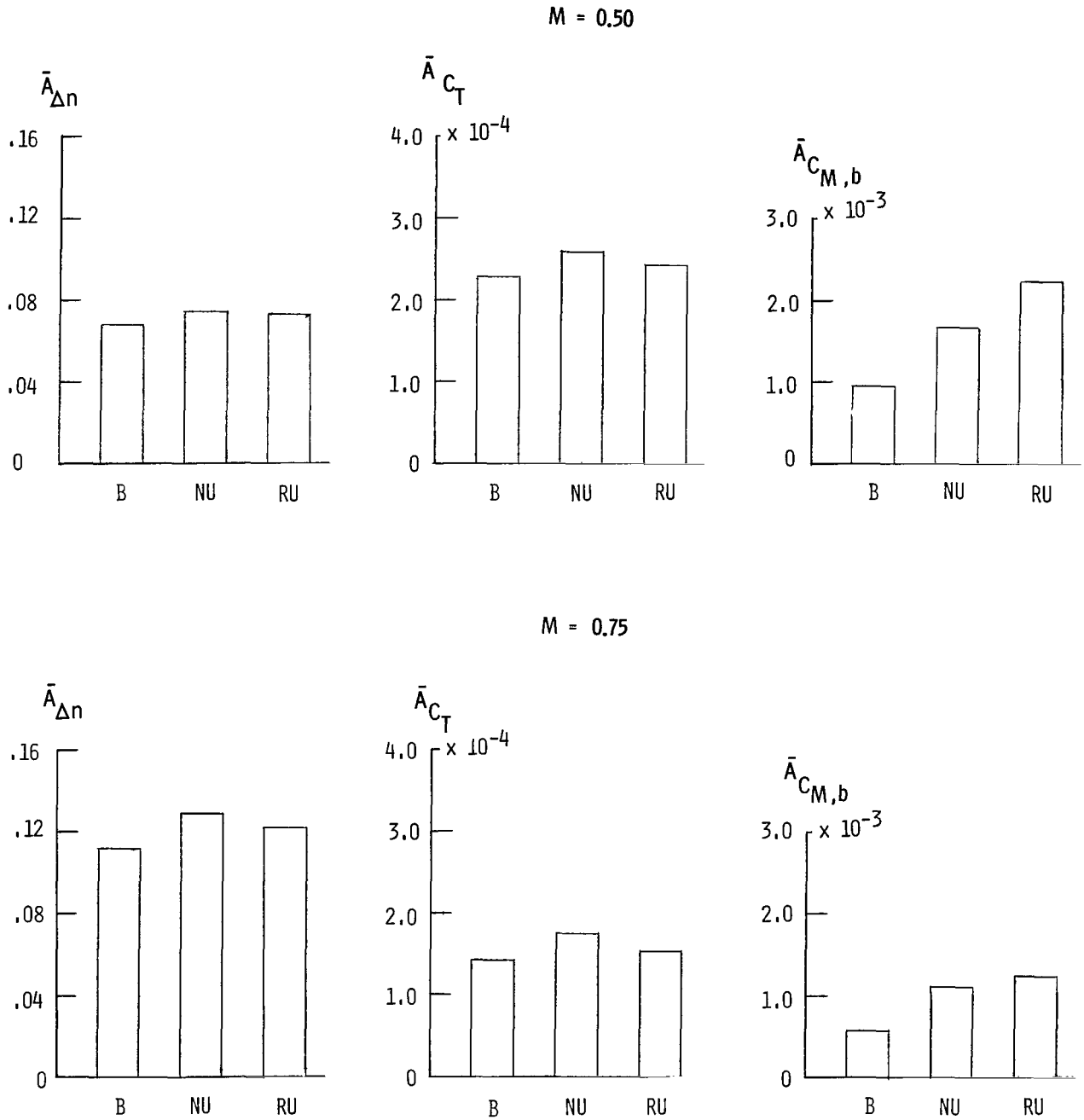

(a) Control law 1.

Figure 10.- Turbulence responses for baseline, nominal-unstable, and reduced-unstable configurations.

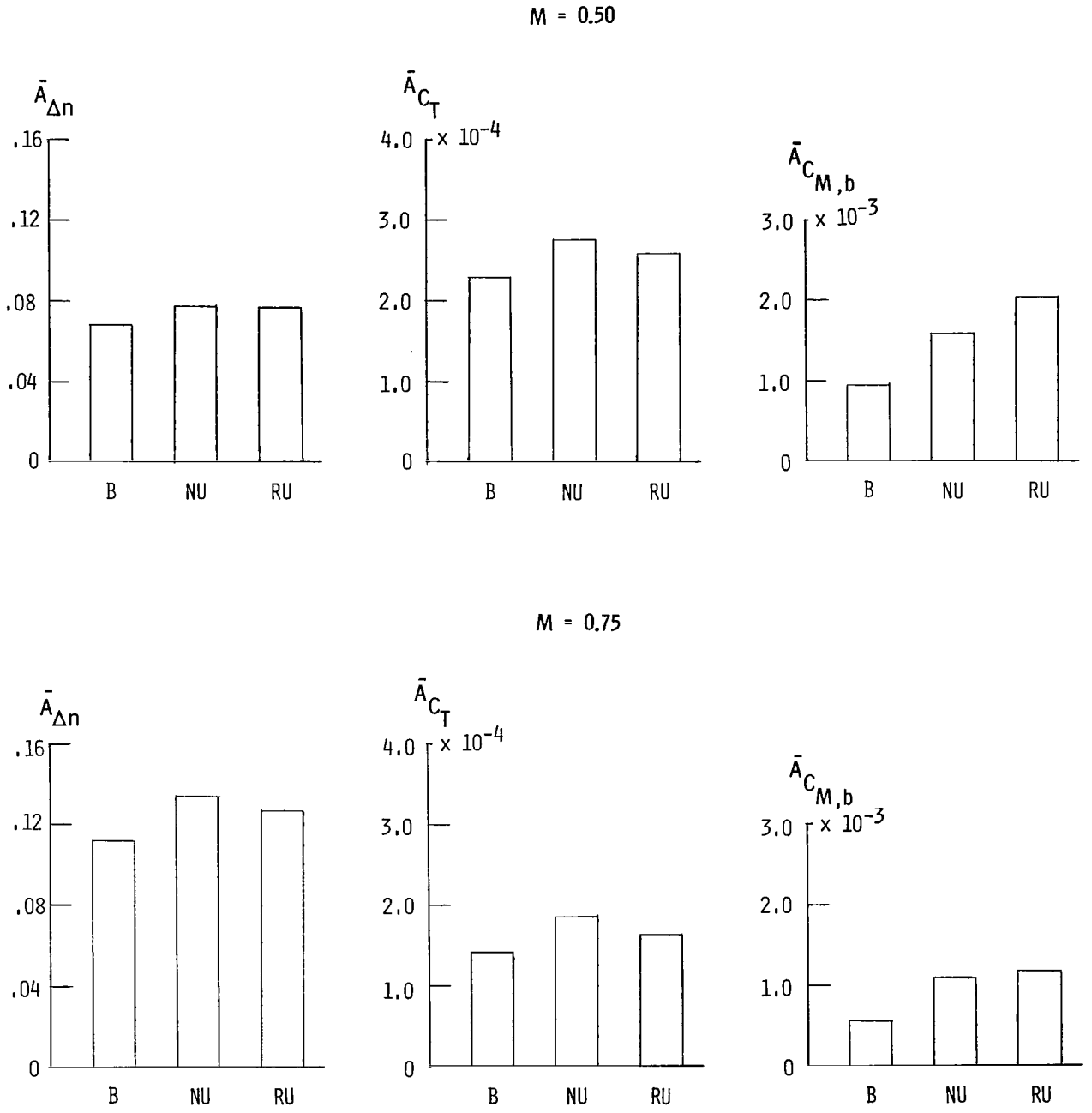

(b) Control law 2.

Figure 10.- Continued.

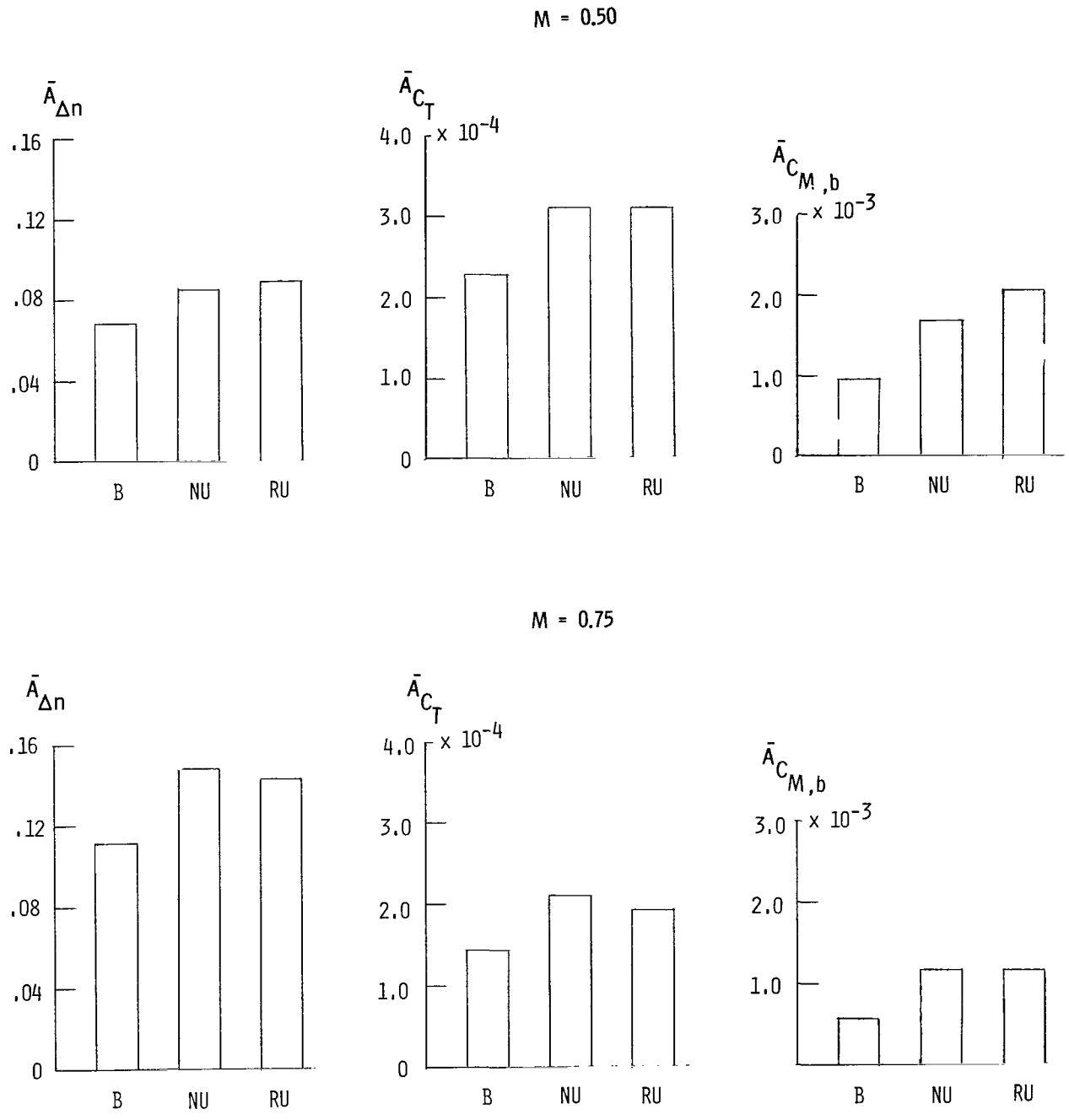

(c) Control law 3.

Figure 10.- Concluded.

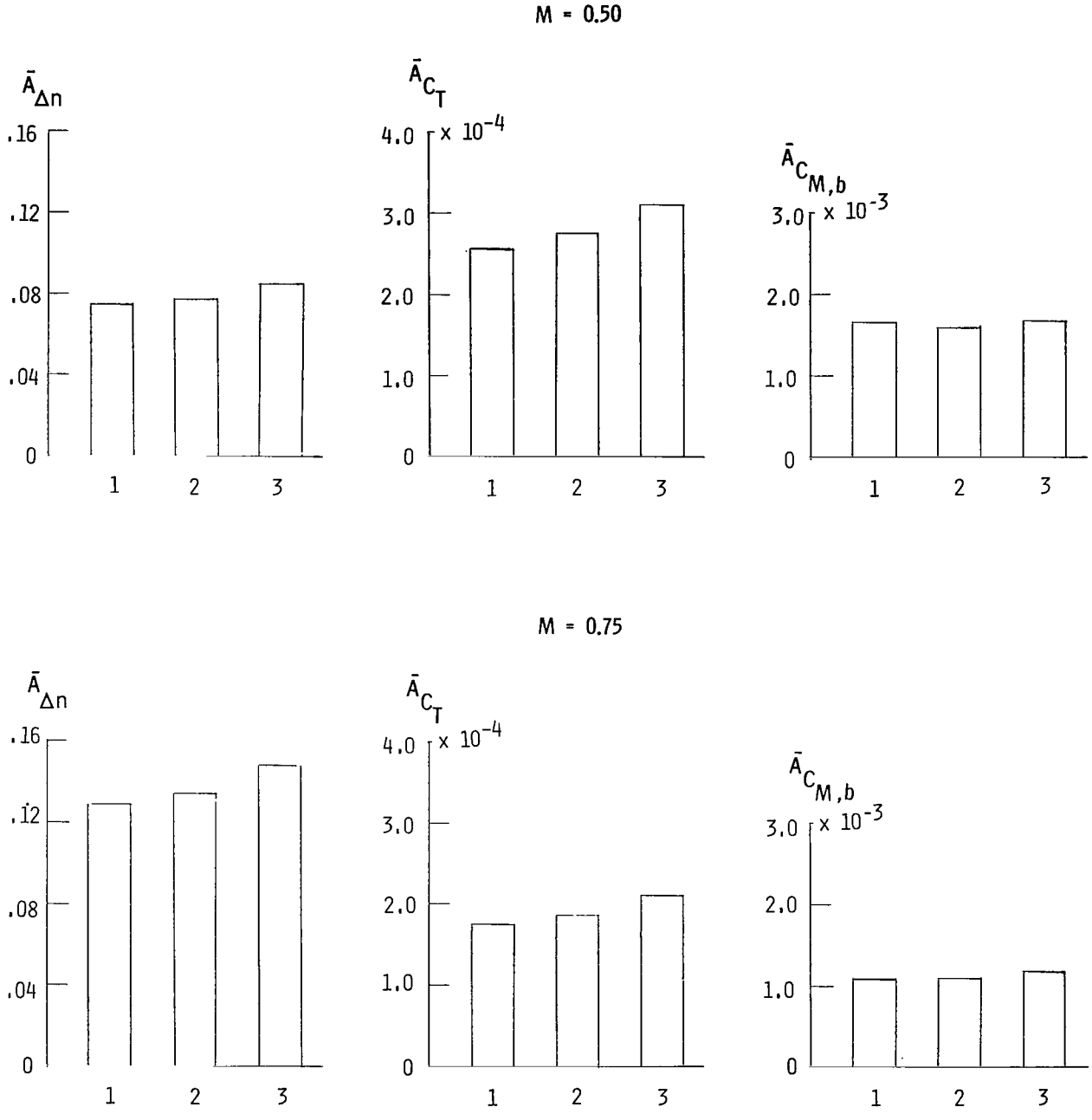

(a) Nominal-unstable configuration.

Figure 11.- Turbulence responses for control laws 1, 2, and 3.

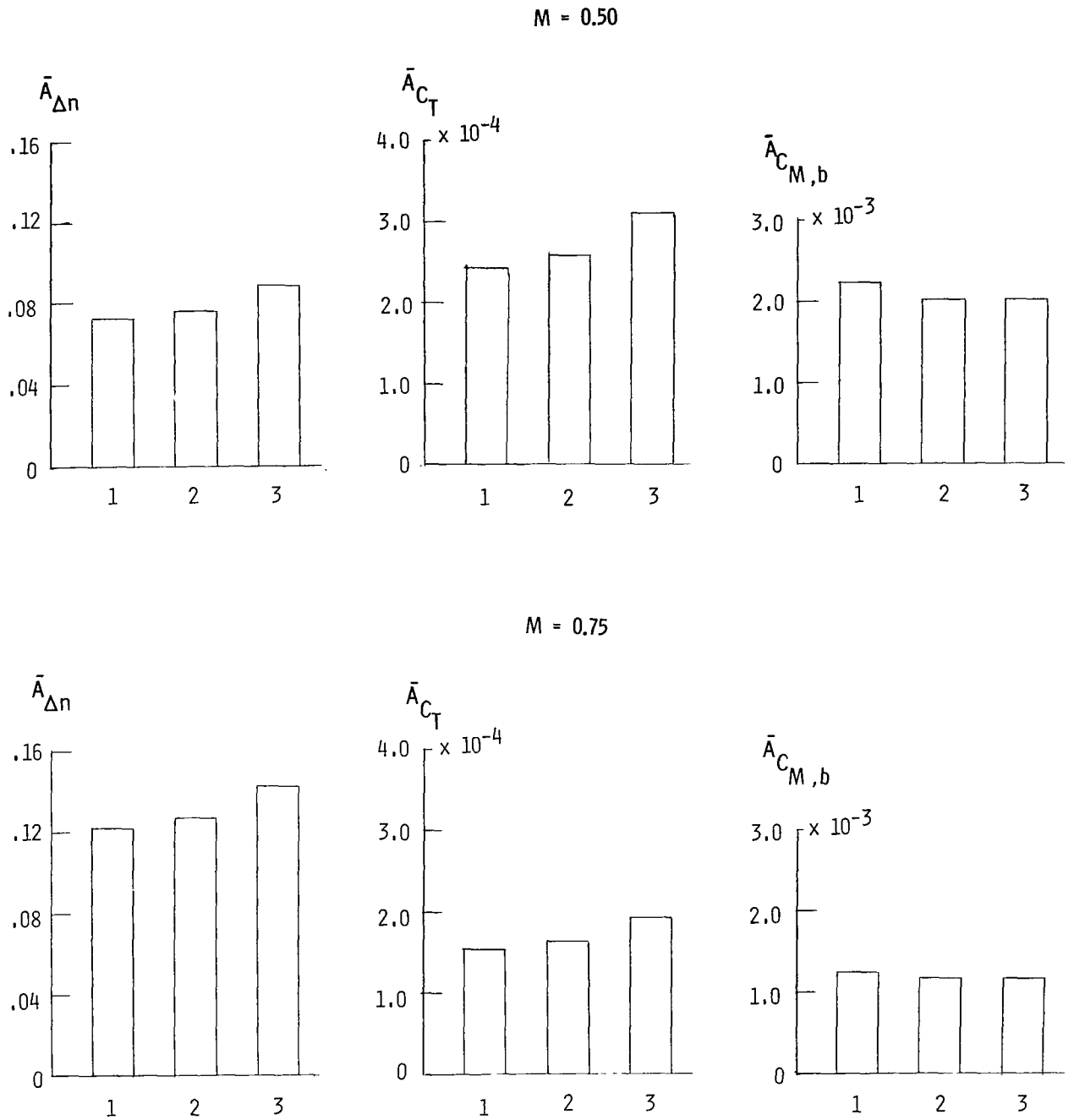

(b) Reduced-unstable configuration.

Figure 11.- Concluded.

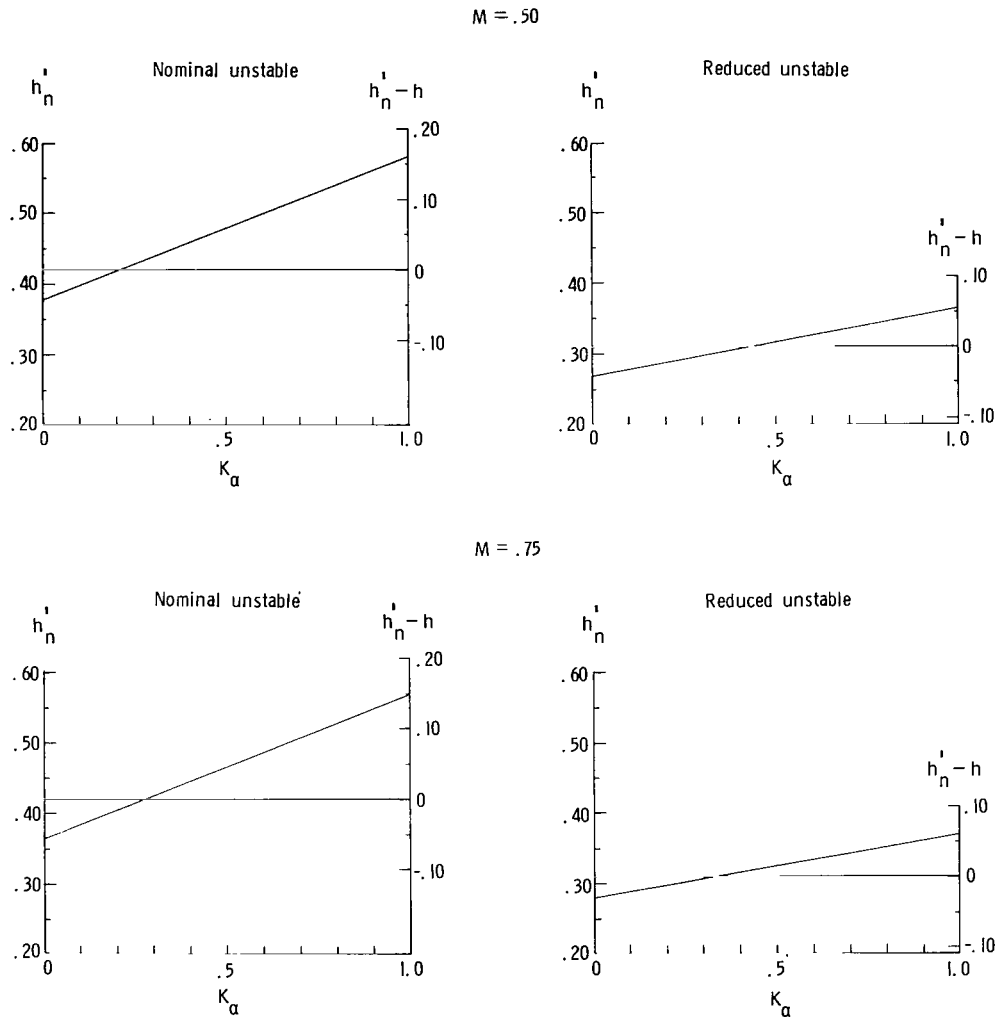

Figure 12.- Effect of angle-of-attack feedback gain on effective neutral point.

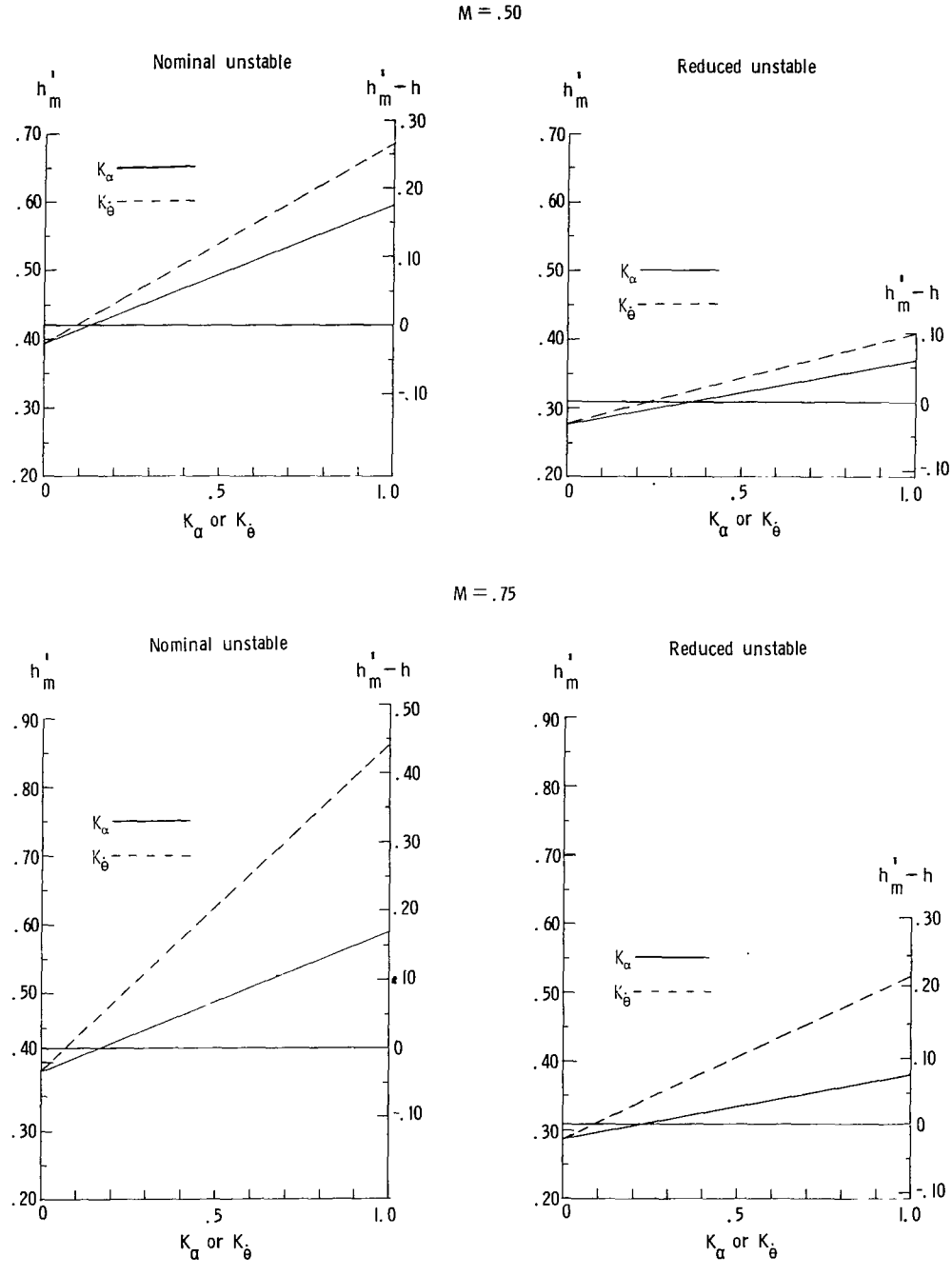

Figure 13.- Effects of angle-of-attack feedback gain and pitch-rate feedback gain on effective maneuver point.

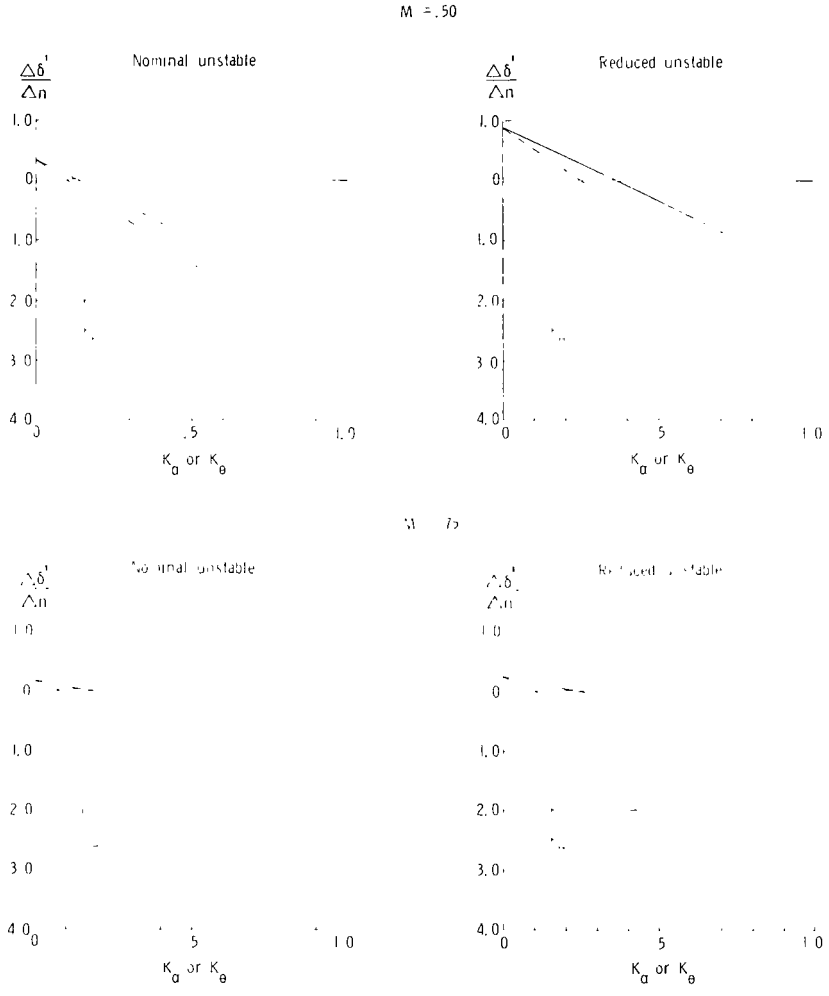

Figure 14.- Effects of angle-of-attack feedback gain and pitch-rate feedback gain on effective elevator angle per g.

NATIONAL AERONAUTICS AND SPACE ADMINISTRATION
WASHINGTON, D.C. 20546

OFFICIAL BUSINESS
PENALTY FOR PRIVATE USE $300

SPECIAL FOURTH-CLASS RATE BOOK

POSTAGE AND FEES PAID
NATIONAL AERONAUTICS AND SPACE ADMINISTRATION
451

U.S.MAIL

POSTMASTER: If Undeliverable (Section 158 Postal Manual) Do Not Return

"The aeronautical and space activities of the United States shall be conducted so as to contribute . . . to the expansion of human knowledge of phenomena in the atmosphere and space. The Administration shall provide for the widest practicable and appropriate dissemination of information concerning its activities and the results thereof."

—NATIONAL AERONAUTICS AND SPACE ACT OF 1958

NASA SCIENTIFIC AND TECHNICAL PUBLICATIONS

TECHNICAL REPORTS: Scientific and technical information considered important, complete, and a lasting contribution to existing knowledge.

TECHNICAL NOTES: Information less broad in scope but nevertheless of importance as a contribution to existing knowledge.

TECHNICAL MEMORANDUMS: Information receiving limited distribution because of preliminary data, security classification, or other reasons. Also includes conference proceedings with either limited or unlimited distribution.

CONTRACTOR REPORTS: Scientific and technical information generated under a NASA contract or grant and considered an important contribution to existing knowledge.

TECHNICAL TRANSLATIONS: Information published in a foreign language considered to merit NASA distribution in English.

SPECIAL PUBLICATIONS: Information derived from or of value to NASA activities. Publications include final reports of major projects, monographs, data compilations, handbooks, sourcebooks, and special bibliographies.

TECHNOLOGY UTILIZATION PUBLICATIONS: Information on technology used by NASA that may be of particular interest in commercial and other non-aerospace applications. Publications include Tech Briefs, Technology Utilization Reports and Technology Surveys.

Details on the availability of these publications may be obtained from:

SCIENTIFIC AND TECHNICAL INFORMATION OFFICE

NATIONAL AERONAUTICS AND SPACE ADMINISTRATION

Washington, D.C. 20546